frontiers | Frontiers in Immunology

TYPE Original Research
PUBLISHED 15 May 2025
DOI 10.3389/fimmu.2025.1594879

OPEN ACCESS

EDITED BY
Zhe Pei,
Virginia Tech, United States

REVIEWED BY
Peng Luo,
Southern Medical University, China
Qihang Yuan,
Dalian Medical University, China
Kan Li,
The State University of New Jersey, United States

*CORRESPONDENCE
Hao Chi
chihao@swmu.edu.cn
Bo Li
liboer2002@swmu.edu.cn
Xiaolin Zhong
xiaolinzhong@swmu.edu.cn

†These authors have contributed equally to this work

RECEIVED 17 March 2025
ACCEPTED 24 April 2025
PUBLISHED 15 May 2025

CITATION
Hu Q, Chen J, Liu Y, Chen H, Lai H, Jiang L, Zhou X, Zhang S, Huang J, Chi H, Li B and Zhong X (2025) TSPAN4$^+$ fibroblasts coordinate metastatic niche assembly through migrasome-driven metabolic reprogramming and stromal-immune crosstalk in pancreatic adenocarcinoma. *Front. Immunol.* 16:1594879. doi: 10.3389/fimmu.2025.1594879

TSPAN4$^+$ fibroblasts coordinate metastatic niche assembly through migrasome-driven metabolic reprogramming and stromal-immune crosstalk in pancreatic adenocarcinoma

Qingwen Hu[1,2†], Jiali Chen[3†], Yang Liu[2,4†], Haiqing Chen[1], Haotian Lai[1], Lai Jiang[1], Xuancheng Zhou[1], Shengke Zhang[1], Jinbang Huang[1], Hao Chi[1*], Bo Li[2*] and Xiaolin Zhong[5*]

[1]Clinical Medical College, Southwest Medical University, Luzhou, China, [2]Department of General Surgery (Hepatopancreatobiliary Surgery), The Affiliated Hospital of Southwest Medical University, Luzhou, China, [3]Department of Oncology, Jinniu District People's Hospital, Chengdu, China, [4]Department of Hepatobiliary Surgery, Zizhong People's Hospital, Neijiang, China, [5]Department of Gastroenterology, The Affiliated Hospital of Southwest Medical University, Luzhou, China

Background: Pancreatic cancer (PC) is a highly aggressive pancreatic malignant tumor with poor prognosis due to its complex tumor microenvironment (TME) and metastatic potential. Fibroblasts play an important role in tumor progression and metastasis by remodeling the extracellular matrix (ECM) and influencing the immune response. This study explored migrasome-associated fibroblasts, especially TSPAN4 and ITGA5, as key regulators of pancreatic cancer metastasis, aiming to provide new ideas for therapeutic strategies targeting TME.

Methods: We employed single-cell RNA sequencing (scRNA-seq) and spatial transcriptomics to analyze pancreatic cancer tissues. Data from the GEO and TCGA databases were integrated and processed using batch correction techniques. Single-cell data were analyzed with Seurat and Monocle for dimensionality reduction and pseudotime trajectory analysis. Cell communication was assessed using CellCall and CellChat. Spatial transcriptomic analysis was conducted with RCTD and MISTy tools to investigate cell interactions within the TME. Additionally, gene enrichment, deconvolution, and prognostic analyses were performed, alongside experimental validation through siRNA transfection, qRT-PCR, and various functional assays to investigate the role of TSPAN4 in metastasis.

Results: Our results underscore the critical role of TSPAN4$^+$ fibroblasts in pancreatic cancer. These fibroblasts were predominantly located at the tumor periphery and exhibited elevated migrasome gene expression, which was associated with enhanced ECM remodeling and immune suppression. Intercellular communication analysis revealed that TSPAN4$^+$ fibroblasts engaged in extensive interactions with immune cells, such as macrophages and endothelial cells, facilitating metastasis and immune evasion. Moreover, the high expression of immune checkpoint markers indicated their involvement in modulating the immune response.

Conclusion: TSPAN4^{+} fibroblasts are key regulators of pancreatic cancer progression, contributing to metastasis, immune suppression, and ECM remodeling. Targeting these fibroblasts represents a promising therapeutic strategy to improve clinical outcomes and enhance the effectiveness of immunotherapies in pancreatic cancer.

KEYWORDS

single-cell analysis, pancreatic ductal adenocarcinoma, immunotherapy, migrasomes, TSPAN4

1 Introduction

Pancreatic carcinoma maintains its status as one of oncology's most formidable malignancies, distinguished by dismal survival metrics and recalcitrance to established treatment paradigms (1, 2). While advancements in early detection methodologies and therapeutic interventions have been achieved, longitudinal survival analyses continue to document persistently suboptimal five-year survival rates. This therapeutic impasse originates fundamentally from the pathobiological complexity inherent in TME dynamics coupled with the malignancy's propensity for systemic dissemination (3–5). The metastatic proclivity of pancreatic neoplasms—manifested through colonization of distant organ systems—emerges as the principal driver of mortality, yet the molecular orchestrators mediating this multi-step metastatic continuum demand further mechanistic clarification (6).

The TME serves as a critical regulatory axis in pancreatic oncogenesis, governed through bidirectional molecular cross-talk between malignant epithelia and stromal constituents, including fibroblasts, immune infiltrates, and vascular networks (7). Emerging evidence suggests that such intercellular communication networks fuel cellular adaptability, particularly the phenotypic reprogramming of quiescent fibroblasts into activated CAF phenotypes during malignant progression (8). These activated stromal components exhibit bifunctional pathological capabilities: fostering neoplastic expansion via growth factor cascades while concurrently facilitating immune escape through matrix reorganization and immunoregulatory factor secretion—processes that synergistically enhance metastatic competence (9). These reciprocal interactions highlight the critical need to characterize fibroblast-derived molecular determinants and their associated signaling pathways, offering promising avenues for disrupting protumorigenic microenvironmental niches through precision therapeutic modalities (10).

Emerging research has elucidated the central regulatory function of migrasomes—dynamic membrane-bound organelles coordinating cellular locomotion—in metastatic pathophysiology (11). Characterized by their molecular composition rich in adhesion regulators and signaling mediators, these subcellular entities facilitate critical microenvironmental crosstalk through spatially organized vesicular trafficking (12). Within the migrasome-associated genetic repertoire, TSPAN4 and ITGA5 emerge as critical effectors governing fibroblast activation dynamics and stromal communication networks, particularly within pancreatic tumor ecosystems (11). The tetraspanin protein TSPAN4 modulates cellular adhesive properties and mechanotransduction pathways, whereas ITGA5—a core component of fibronectin-binding integrin complexes—mediates extracellular matrix anchorage and migratory programming through focal adhesion kinase activation (13, 14).

This investigation systematically examines the pathophysiological contributions of migrasome-associated fibroblast subpopulations to metastatic dissemination in pancreatic malignancies, with particular emphasis on TSPAN4/ITGA5 expression gradients across tumor ecosystem compartments. We mechanistically dissect these biomarkers' regulatory roles in disease progression through an integrated multi-omics approach. Employing scRNA-seq coupled with spatial transcriptomic profiling, our experimental paradigm deciphers spatiotemporal interaction networks among stromal fibroblasts, immune effectors, and vascular components, establishing quantitative associations between intercellular crosstalk dynamics and metastatic outcomes (15). By synthesizing transcriptional signatures, ligand-receptor spatial mapping, and microenvironmental architecture analysis, this multiplexed analytical framework unveils previously unrecognized regulatory hierarchies within pancreatic TME and proposes druggable targets for precision stromal modulation (16).

2 Materials and methods

2.1 Genomic data curation and integration

Single-cell transcriptomic profiles were sourced from the GEO repository (Accession: GSE197177), comprising three clinical cohorts: primary pancreatic carcinoma specimens (GSM5910784, GSM5910787), hepatic metastatic lesions (GSM5910785, GSM5910788), and non-malignant pancreatic tissues (GSM5910786). Spatial transcriptomic datasets (GSM7498811,

GSM7498813) were concurrently extracted for tumor microenvironmental architecture analysis. Clinical annotation-matched RNA-seq data for 178 pancreatic ductal adenocarcinoma cases were procured from TCGA (National Cancer Institute Genomic Data Commons). To address technical variability across platforms, cross-dataset normalization was conducted via the "limma"(3.60.3) (17) and "sva"(3.52.0) (18) computational frameworks in R.

2.2 Transcriptomic signature quantification

The GSE132257 scRNA-seq dataset was curated and interrogated through the "Seurat"(5.1.0) computational framework (19). Initial quality control retained 28,912 high-confidence cells from a raw dataset of 35,487 cells after applying thresholds: mitochondrial gene content <10% (percent.mt < 10), unique gene counts between 200 and 2,500 (nFeature_RNA > 200 & nFeature_RNA < 2500). Following multi-algorithmic dimensional compression—implementing principal component analysis (PCA) for feature extraction with subsequent visualization via t-SNE and UMAP projection (20) —we identified high-variance transcripts (top 2000 genes) for cellular clustering and phenotypic characterization (21). Five complementary scoring paradigms (AUCell, UCell, singscore, GSEA, AddModuleScore) were systematically implemented for pathway activity quantification (22). Comparative module score analyses across defined cellular clusters were conducted using nonparametric statistical approaches.

2.3 Cellular trajectory reconstruction and signaling network mapping

Our analytical pipeline incorporated "monocle"(2.32.0) (23–25) and "Seurat" (5.1.0) frameworks (20) for fibroblast-specific transcriptomic interrogation. After quality filtering and stromal cell population isolation, we constructed CellDataSet architectures to calculate transcriptional variability metrics (26). High-confidence genes meeting dual thresholds (expression magnitude & dispersion variance) underwent DDRTree-based manifold learning (27) for nonlinear dimensional reduction. Quasitemporal ordering algorithms reconstructed cellular ontogeny trajectories (28), with trajectory heatmaps and state projection plots delineating fibroblast phenotypic evolution within tumor niches (29). Intercellular signaling dynamics were decoded through CellCall/CellChat platforms (30, 31), enabling systematic identification of ligand-receptor interplay across microenvironmental compartments.

2.4 Spatial metabolic profiling in pancreatic ecosystems

Spatial metabolomic analysis of pancreatic tumor architecture was performed using integrated computational workflows. After stringent quality control—including removal of mitochondrial transcripts and selection of ribosomal protein-coding genes—raw sequencing data were normalized using SCTransform. Dimensionality reduction was conducted via PCA, followed by UMAP for cluster identification (32). SpatialFeaturePlot algorithms mapped transcriptomic gradients across tissue microdomains (33), while "scMetabolism"(0.2.1) quantified pathway activation states through enzyme-centric scoring. DotPlot visualizations highlighted metabolic heterogeneity across cellular compartments (34), complemented by spatiotemporally resolved heatmaps delineating pathway-associated gene distributions within tumor topographies.

2.5 Discriminative gene identification and functional annotation

Our analytical cascade implemented a multi-stage computational pipeline for spatial transcriptomic feature extraction and pathway enrichment. Following rigorous preprocessing protocols (gene filtration, read depth normalization, logarithmic conversion, and expression standardization) (35, 36), principal component analysis (PCA) facilitated feature space compression and discriminative gene identification. Topological cell neighborhood mapping through K-nearest neighbors (KNN) algorithms preceded community detection via Louvain-Leiden clustering paradigms (37). Correlation-driven gene prioritization employing Spearman's rank metrics identified statistically significant ($p<0.05$) positive/negative transcriptional regulators, subsequently subjected to pathway enrichment interrogation via Metascape's bioinformatics suite (38, 39).

2.6 Spatial omics interrogation via RCTD-MISTy frameworks

We implemented a dual-algorithm spatial omics pipeline ("RCTD"/"MISTy") to decode multicellular interactomes in pancreatic malignancies (40, 41). Initial scRNA-seq curation involved systematic cell type classification to generate reference cellular atlases. Spatial transcriptomic inputs underwent topological parsing through RNA localization mapping and marker colocalization profiling. The "RCTD" computational framework (41) enabled probabilistic cell type deconvolution by integrating single-cell references with spatial resolution data. For microenvironmental crosstalk mapping, the "MISTy" platform (40) quantified intercellular signaling across defined spatial domains (intra-tumoral, juxta-tumoral, para-tumoral), generating multiplexed interaction matrices and spatially resolved ligand-receptor activation heatmaps.

2.7 Cellular composition deconvolution and trajectory modeling

Our analytical framework integrated scRNA-seq and spatial transcriptomic (stRNA-seq) datasets for cellular topology

reconstruction and temporal dynamics inference. Fibroblast subpopulations were computationally isolated from annotated single-cell repositories and stratified into TSPAN4+/- cohorts based on transmembrane protein expression thresholds. Transcriptomic profiles underwent format standardization via "SingleCellExperiment" object conversion, followed by rigorous preprocessing (count normalization, low-abundance ribosomal/mitochondrial transcript filtration). The "SPOTlight"(1.8.0) (42) deconvolution engine enabled cellular spatial mapping through integrative analysis of single-cell and spatial resolution data, employing randomized subsampling (n=100 per cell type) to optimize computational tractability. High-confidence markers (AUC>0.7) were prioritized for spatial pattern validation using Seurat's visualization modules (25), while "monocle" (2.32.0) (23, 24) pseudotemporal ordination algorithms reconstructed cellular transition trajectories.

2.8 Spatial architecture mapping and clinical prognostication

Our analytical pipeline implemented the "spacexr" (v2.2.1) computational framework (41) for spatial deconvolution coupled with multi-modal prognostic modeling. Stromal fibroblasts were computationally segregated from scRNA-seq repositories and stratified into TSPAN4-expressing versus null subpopulations. Reference spatial atlases were constructed using "spacexr"'s probabilistic modeling architecture, enabling high-resolution mapping of fibroblast spatial topographies within tumor microdomains. Complementarily, bulk transcriptomic infiltration profiling and survival prognostication were executed through TSPAN4+ fibroblast marker-derived signatures. Pathway dysregulation was quantified via "GSVA" (1.52.3) enrichment scoring (43), with parallel evaluations of immunotherapy responsiveness and survival correlations conducted through multivariate Cox regression modeling.

2.9 RNA interference and cellular model preparation

Human pancreatic adenocarcinoma cell lines (SW1990, PANC-1) were maintained in DMEM culture medium containing 10% heat-inactivated FBS and antibiotic-antimycotic solution (100 U/mL penicillin, 100 μg/mL streptomycin). Gene silencing experiments employed TSPAN4-specific siRNA (si-TSPAN4) or scrambled control siRNA (si-NC) delivered via GA-DNA Transfection Reagent (GeneAdv Co., Suzhou), following the manufacturer's protocol. Post-transfection cellular models were subjected to a 48-hour incubation period prior to downstream functional assays.

2.10 Transcript quantification via qRT-PCR

Total RNA was isolated employing TRIzol reagent (Thermo Fisher Scientific), followed by reverse transcription into cDNA using PrimeScript RT Master Mix (Takara Bio Inc.). Amplification reactions were conducted using the Applied Biosystems 7500 platform with SYBR Green chemistry (Takara Bio Inc.), utilizing *GAPDH* as an endogenous control. TSPAN4 mRNA levels were determined through comparative threshold cycle analysis, with normalized expression levels computed via the ΔΔCt ($2^{-\Delta\Delta Ct}$) algorithm.

2.11 Cellular proliferation kinetics assessment

Proliferative dynamics were quantified using the CCK-8 assay system (Dojindo Molecular Technologies). SW1990 and PANC-1 cellular models were plated in 96-well microtiter plates (1.5×10^3 cells/well) and subjected to temporal monitoring at 24-hour intervals (24-96h) post-transfection. Following each incubation epoch, CCK-8 chromogenic solution (10μL/well) was introduced, with subsequent spectrophotometric quantification (450nm wavelength) performed using a multi-mode microplate reader to determine relative proliferative indices.

2.12 Clonogenic potential evaluation

The clonogenic capacity of SW1990 and PANC-1 cellular models was evaluated through 6-well plate assays (500 cells/well). Following 14-day incubation under standard culture conditions, clonogenic units were chemically immobilized with 4% paraformaldehyde and chromatically labeled with 0.1% crystal violet solution. Quantitative analysis of colony formation efficiency was performed through digital image processing using ImageJ's automated enumeration algorithms.

2.13 *In vitro* migratory capacity assessment

Cellular migratory potential was analyzed through a standardized scratch assay. SW1990 and PANC-1 cell monolayers were established in 6-well culture plates until achieving 90% confluency. Mechanical wound induction was performed using sterile 200 μL pipette tips, followed by sequential image acquisition at baseline (0 h) and 48 h post-wounding using an Olympus IX73 inverted phase-contrast microscope system. Wound closure kinetics were computationally quantified via ImageJ's MRI Wound Healing Tool plugin for normalized metric derivation.

2.14 *In vitro* invasive capacity profiling

Cellular invasiveness was evaluated using Matrigel-coated Transwell systems (8μm pore, Corning Inc.). Post-transfection cellular cohorts (si-TSPAN4 vs. scrambled siRNA controls) were suspended in serum-free medium (2×10^4 cells/insert) within upper chambers, while lower compartments contained chemoattractant-

enriched medium (10% FBS). Following 24-hour chemotactic induction at 37°C/5% CO_2, non-invasive cellular fractions were mechanically cleared from upper membranes. Transmigrated cell populations were chemically immobilized (4% paraformaldehyde), chromatically labeled (0.1% crystal violet), and quantified through microscopic enumeration (5 randomized high-power fields). Invasion indices were calculated by normalizing experimental group transmigration counts against control baselines.

2.15 Apoptotic profiling via flow cytometry

Programmed cell death quantification was performed using the Annexin V-FITC/PI Apoptosis Detection System (BD Biosciences). Post-transfection cellular cohorts (si-TSPAN4 vs. scrambled siRNA controls) were harvested at 48h, subjected to dual PBS rinses, and dual-stained with Annexin V-FITC/PI fluorophores. Cellular fluorescence profiles were acquired via a BD FACSCanto II analytical cytometer, with apoptotic indices (encompassing both initial and terminal phases) computationally derived through FlowJo™ v10.8.1 multiparametric analysis suites.

2.16 Statistical analysis

Statistical analyses were performed using R software (version 4.4.1). Data from the GEO and TCGA databases underwent quality control and batch effect correction. Various computational approaches were employed for dimensionality reduction, data visualization, gene set scoring, pseudotime trajectory inference, intercellular communication analysis, spatial transcriptomics, and prognostic evaluation. Experimental validation was conducted to confirm the findings. Statistical significance was defined as p-values and false discovery rate (FDR) q-values < 0.05. These methodologies ensured rigorous data processing and analysis, providing insights into the initiation, progression, and metastasis of pancreatic cancer, as well as potential therapeutic targets.

3 Results

The research idea of this study is presented as a flow chart (Figure 1).

3.1 Architectural diversification and metastatic pathway activation in cellular ecosystems

Through t-SNE-optimized transcriptomic cartography, we deconstructed cellular landscapes across three clinical cohorts: non-malignant controls (CT), metastatic carcinoma (MC), and pancreatic adenocarcinoma (PC). Lineage-specific stratification partitioned cell populations via canonical biomarkers, identifying 11 functionally discrete compartments including T cell effectors, ductal epithelia, β-islet clusters, myeloid phagocytes, acinar units, macrophage subtypes, plasmacytoid secretors, stromal fibroblasts, mast cell derivatives, vascular networks, and B lymphocytes (Figure 2A). Quantitative intergroup comparisons unveiled profound divergence in cellular stoichiometry and spatial patterning among CT, MC, and PC specimens (Figure 2B).

Multi-algorithmic pathway activation profiling (AUCell/UCell/singscore/ssGSEA/AddModuleScore) revealed preferential upregulation of prometastatic gene modules within fibroblastic compartments, as evidenced by concordant multi-metric scoring matrices (Figure 2C violin plots). Transcriptional gradient mapping confirmed fibroblast dominance in metastasis-related pathway activation across all analytical platforms. t-SNE projection analysis (Figure 2D) demonstrated compartment-specific spatial segregation of major lineages, with MC/PC stromal fibroblasts and vascular endothelia exhibiting heightened activation states versus CT counterparts.

Differential expression validation identified fibroblast-selective overexpression of TSPAN4/ITGA5 (Figure 2E). UMAP-based spatial transcriptomics (Figure 2F) resolved distinct molecular geographies: TSPAN4 showed niche-restricted expression in fibroblastic zones and ductal interfaces, contrasting with ITGA5's pan-stromal/endothelial distribution. These polarized expression topographies implicate complementary roles in tumor-stromal signaling - TSPAN4 as a focal signaling node versus ITGA5 as a ubiquitous adhesion mediator.

3.2 Migrasome dynamics in fibroblast activation and stromal crosstalk

Migrasome-enriched fibroblast subsets underwent comprehensive characterization through pseudotemporal trajectory reconstruction and intercellular signaling network resolution. Initial trajectory modeling (Figure 3A) mapped the temporal activation of migrasome-related transcriptional programs, pinpointing TSPAN4/ITGA5 as key early-stage mediators during malignant transformation. Phenotypic state transitions along the developmental continuum were visualized through trajectory topology mapping (Figure 3B), revealing progressive lineage diversification. UMAP cluster progression analysis (Figure 3C) documented dynamic fibroblast subset expansion from 17 to 19 distinct phenotypes during disease progression.

Transcriptome-based stratification segregated fibroblasts into migrasome-abundant (MigrasomeHigh-Fibro) and -depleted (MigrasomeLow-Fibro) subgroups. Fibroblasts were classified as MigrasomeHigh-Fibro if their expression of migrasome-associated genes (TSPAN4, ITGA5) exceeded the 75th percentile of all fibroblasts, and as MigrasomeLow-Fibro if below the 25th percentile. Ligand-receptor flux quantification via chordal network mapping (Figure 3D) revealed MigrasomeHigh-Fibro as principal signal transducers, exhibiting preferential communication with tumor-associated macrophages, vascular networks, and ductal interfaces (Figure 3E). Pathway activation stratification (Figure 3F) demonstrated subgroup-specific signaling polarization, with MigrasomeHigh-Fibro displaying marked hyperactivity in PERIOSTIN, non-canonical WNT, COMPLEMENT, FGF, TGFβ,

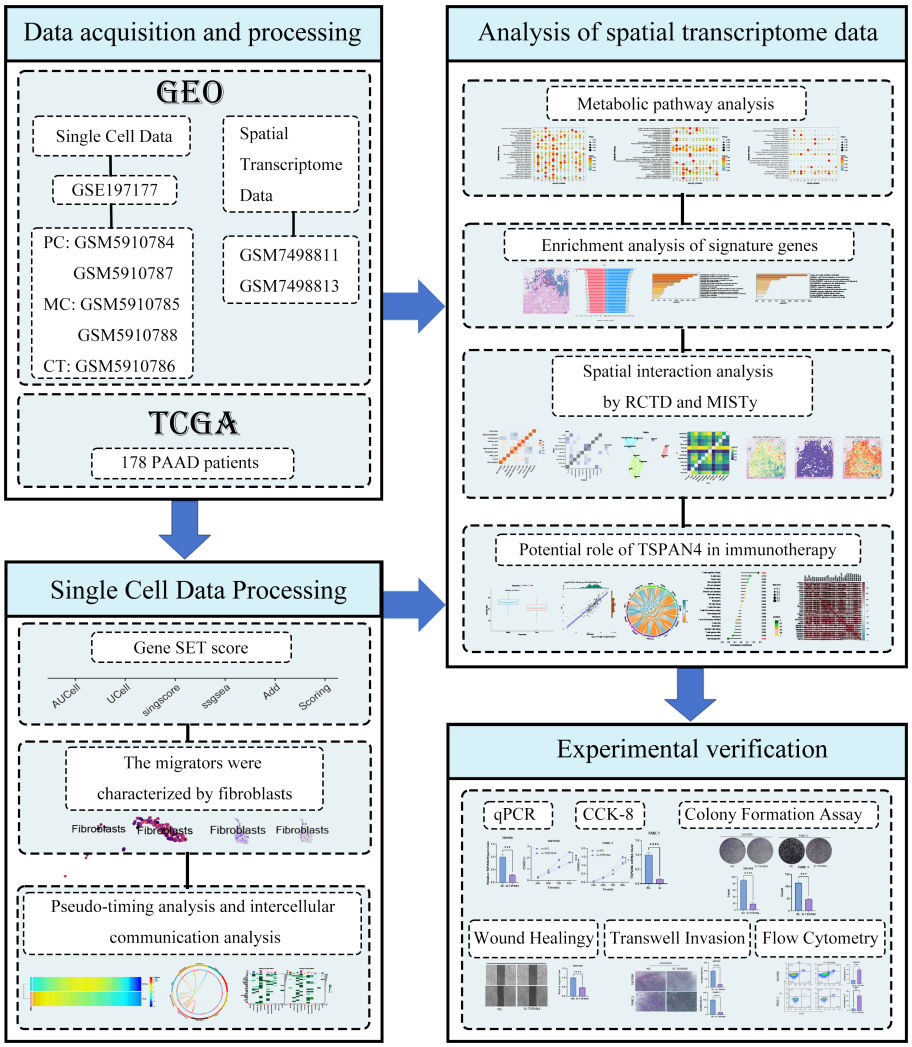

FIGURE 1
Flowchart of the study.

and ANGPTL pathways. Mechanistic dissection (Figure 3G) established MigrasomeHigh-Fibro as central PERIOSTIN network hubs, coordinating pro-metastatic signaling through PI3K/Akt axis activation while concurrently regulating COMPLEMENT/FGF/TGFβ/ANGPTL cascades. CellCall-derived multilayer Sankey network visualization (Figure 3H) decoded the hierarchical architecture of fibroblast-dominated signaling circuits, revealing topological specialization in niche-specific regulatory networks.

3.3 Spatial metabolic circuitry governed by migrasome signaling hubs

Spatial omics mapping unveiled niche-restricted overexpression of migrasome regulators TSPAN4/ITGA5 within specialized tumor microdomains, prompting systematic interrogation of their metabolic network engagement. UMAP-driven manifold learning resolved 14 transcriptionally discrete cellular modules (Figure 4A), with spatial deconvolution algorithms mapping their histoanatomical zonation (Figure 4B). Transcriptional gradient quantification (Figure 4C) identified clusters 4/13/14 as primary reservoirs of TSPAN4/ITGA5 co-expression, demonstrating exceptional cellular penetrance (>80% detection frequency). Metabolic flux profiling (Figure 4D) revealed coordinated activation of bioenergetic networks - particularly oxidative phosphorylation and lipid handling machinery - within migrasome-enriched compartments.

Cross-cohort validation delineated 13 conserved cellular ecotypes (Figure 4E), with spatial zonation cartography (Figure 4F) confirming microniche conservation across specimens. Cluster 13 emerged as the predominant migrasome signaling hub (Figure 4G), exhibiting multi-omic metabolic reprogramming signatures (Figure 4H) through integration of glutaminolysis intermediates and nucleotide biosynthesis precursors. These data position migrasome-active cellular coalitions as metabolic master regulators, synchronizing tumor microenvironmental rewiring via spatiotemporal control of nutrient allocation and anabolic programming.

10.3389/fimmu.2025.1594879

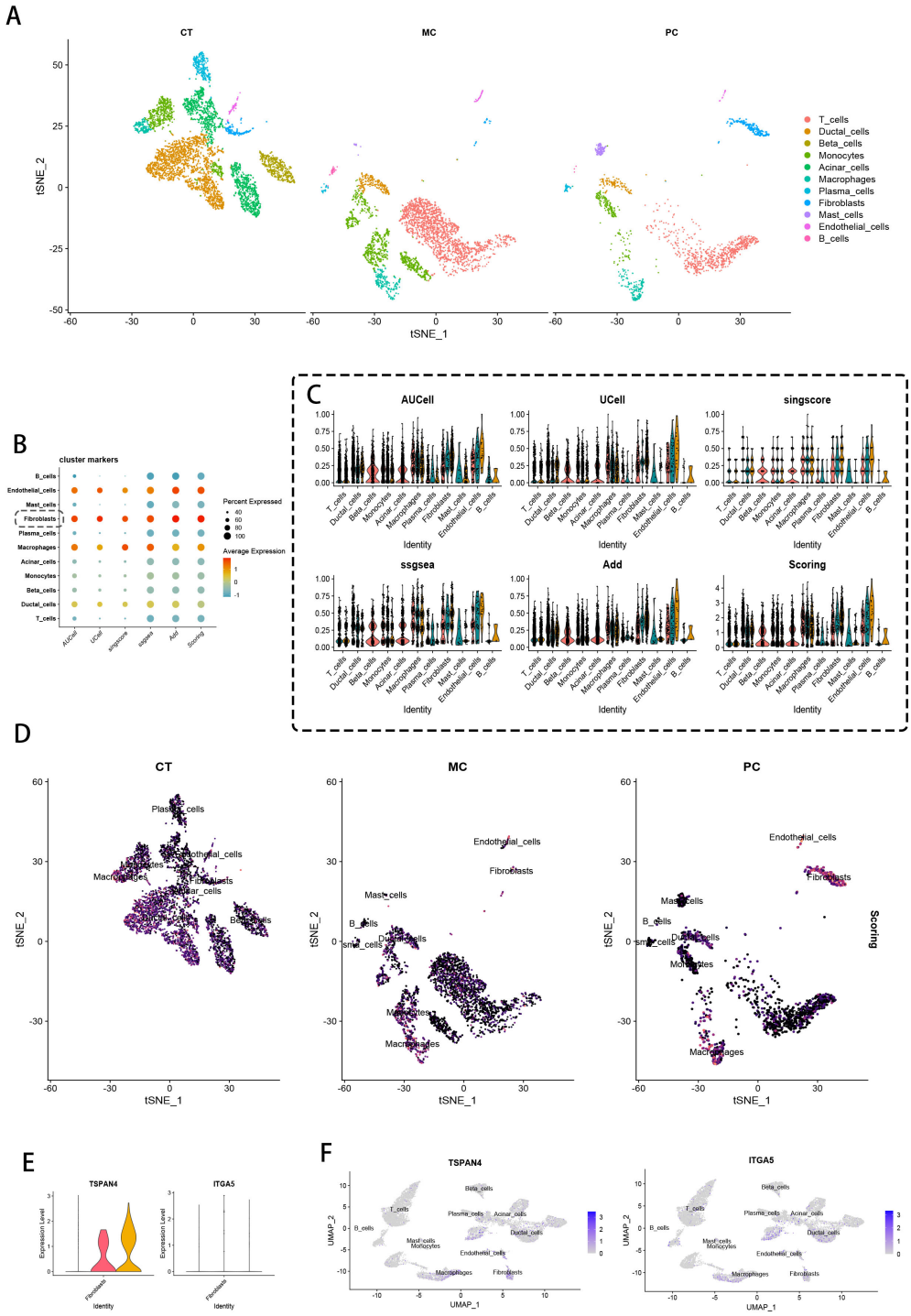

FIGURE 2
Single-cell data processing and scoring. **(A)** t-SNE visualization of single cells from control tissue (CT), metastatic cancer (MC), and primary cancer (PC). **(B)** Heatmaps of migration-related gene expression in different cell clusters, evaluated using AUCell, UCell, and singscore. **(C)** Violin plots detailing the AUCell, UCell, singscore, ssGSEA, and AddModuleScore values in different cell clusters, where each point represents the average expression and the percentage of cells expressing the given marker. **(D)** t-SNE projections of CT, MC, and PC samples highlighting the spatial distribution of major cell types, with color-coded scores reflecting functional activity related to migration traits. **(E)** Violin plots of TSPAN4 and ITGA5 expression. **(F)** UMAP projections of TSPAN4 and ITGA5 expression.

10.3389/fimmu.2025.1594879

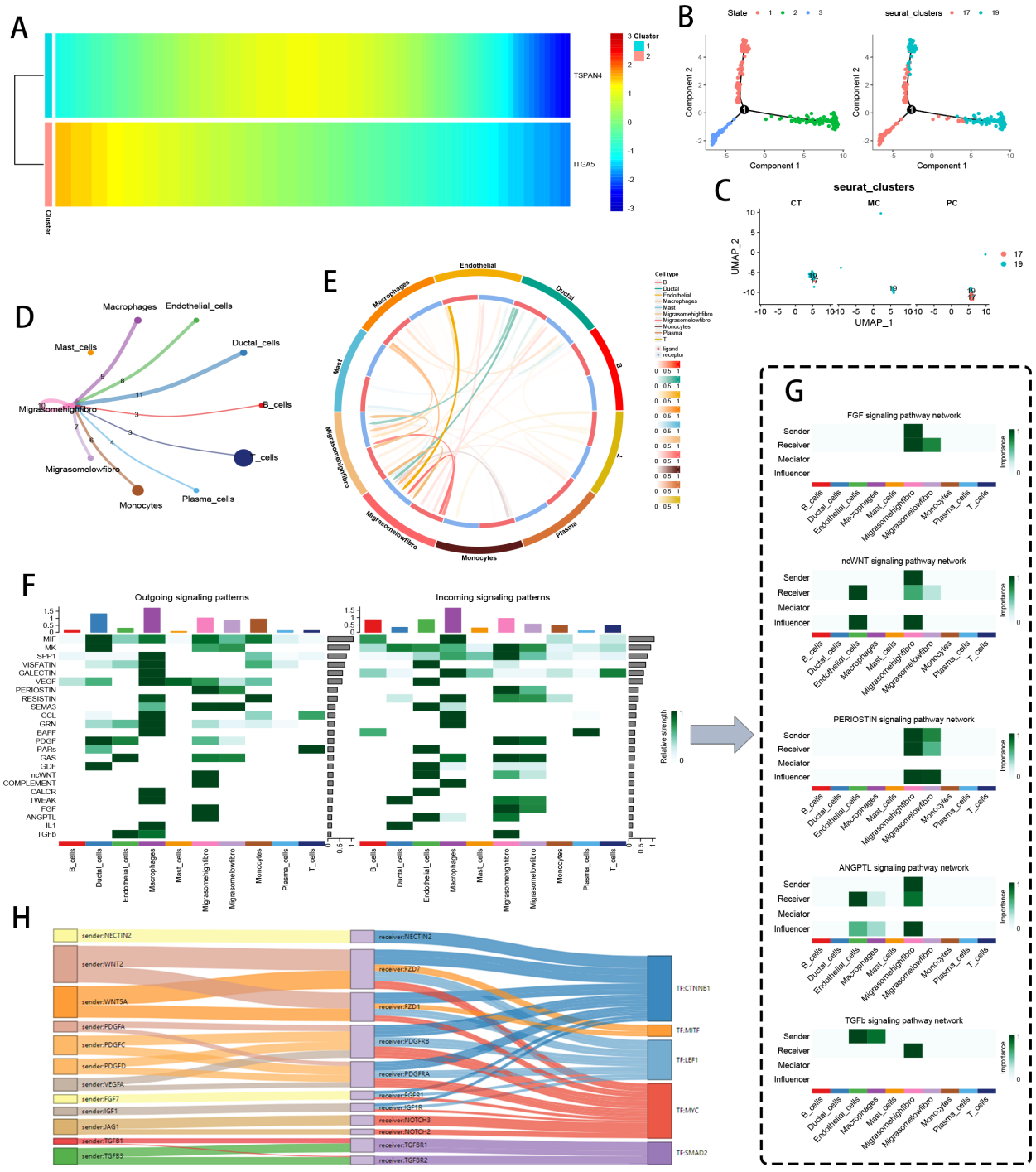

FIGURE 3
Fibroblast pseudotime and communication analysis based on migration traits. **(A)** Pseudotime heatmap showing TSPAN4 and ITGA5 expression during cancer cell progression. **(B)** Trajectory plots of different cell states along pseudotime. **(C)** UMAP plots of fibroblasts from CT, MC, and PC tissues. **(D, E)** Chord diagrams of intercellular communication signals between Migrasome-high fibroblasts and Migrasome-low fibroblasts. **(F)** Heatmap of communication signals (e.g., PERIOSTIN, ncWNT, COMPLEMENT, FGF, THFb, ANGPTL) between different cell clusters. **(G)** Specific Sender, Receiver, Mediator, and Influencer of the PERIOSTIN, ncWNT, Complement, FGF, THFb, and ANGPTL signaling pathways in Migrasome-high and Migrasome-low fibroblasts. **(H)** Sankey diagram of important ligand-receptor pairs involved in communication between Migrasome-high and Migrasome-low fibroblasts.

10.3389/fimmu.2025.1594879

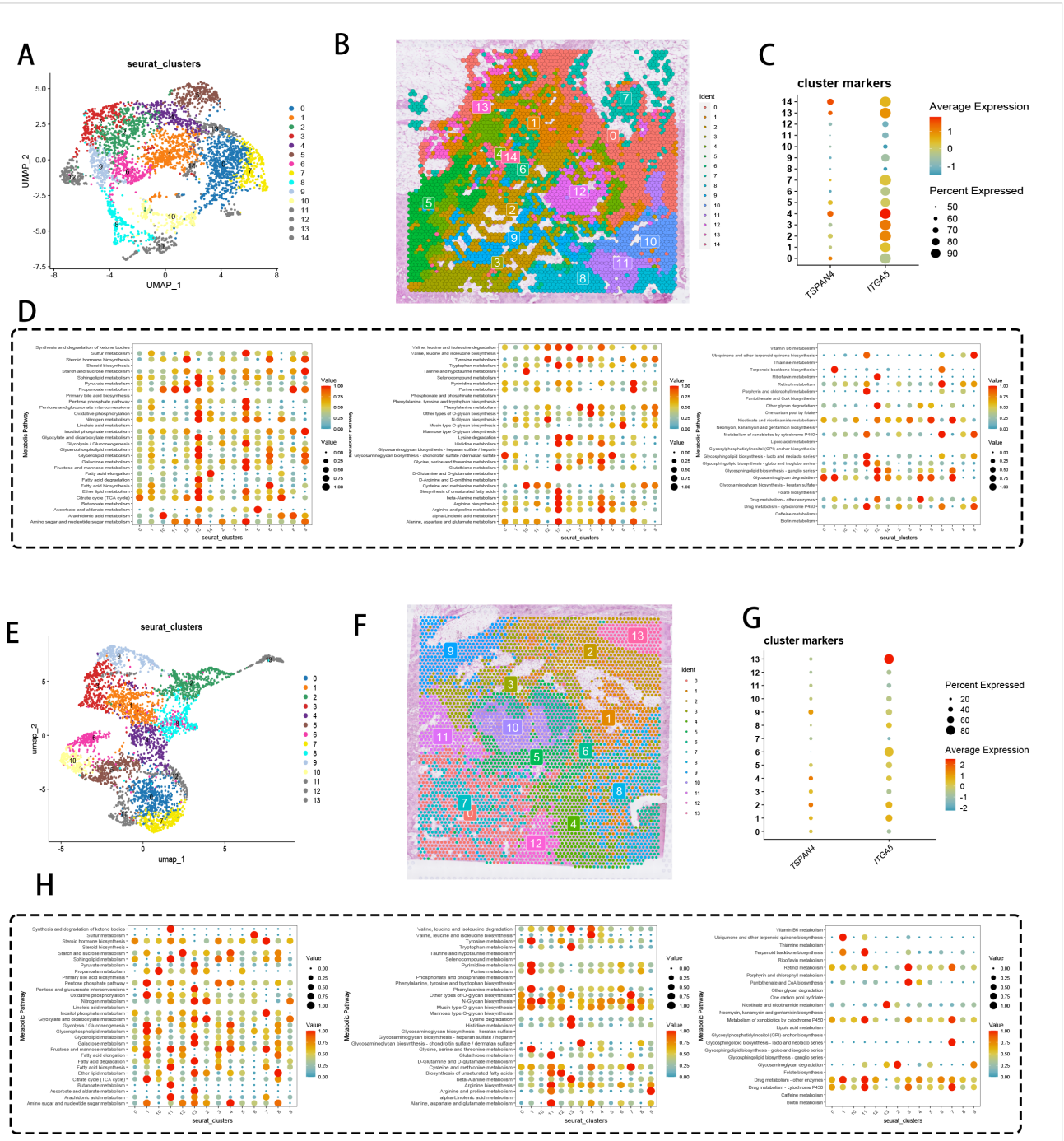

FIGURE 4
Spatial transcriptomics and metabolic analysis. **(A)** UMAP dimensionality reduction showing pancreatic cancer cell clustering. **(B)** Spatial distribution of the 14 clusters within tissue sections. **(C)** DotPlot displaying the average expression levels and percentages of cells expressing TSPAN4 and ITGA5. **(D)** Heatmap of expression levels of different metabolic pathways across cell clusters. **(E)** UMAP dimensionality reduction displaying 13 cell clusters. **(F)** Spatial distribution of the 13 clusters within tissue sections. **(G)** DotPlot showing migration-related gene expression levels and the percentage of cells expressing these genes. **(H)** Heatmap of expression levels in various metabolic pathways across cell clusters.

3.4 Temporal dynamics of spatial transcriptomic programs and pathway hierarchy

Temporal trajectory reconstruction of spatial transcriptomic signatures decoded molecular hierarchies governing ECM remodeling, signaling axis activation, migratory programming, and immune modulation across tumor progression. Cluster 5→0 temporal progression (Figure 5A) identified divergent transcriptional patterning across 30 co-directional and inverse regulatory modules (Figure 5B). Functional enrichment clustering of co-directional modules revealed predominant ECM catabolic pathway activation (Figure 5C), establishing mechanistic linkage to desmoplastic remodeling, invasive niche formation, and PD-L1-

mediated immune evasion. Counter-gradient modules exhibited inverse correlation with MAPK signaling cascades (Figure 5D)—central regulators of proliferative signaling and survival pathways.

Cluster 5→1 trajectory analysis (Figure 5E) uncovered integrin signalosome assemblies as dominant co-directional networks (Figure 5G), while inverse modules governed endosomal trafficking and receptor recycling (Figure 5H). Cluster 8→5 temporal mapping (Figure 5I) exposed interferon-responsive apoptotic regulators as synchronized modules (Figure 5K), opposed by counter-regulated programs controlling ECM

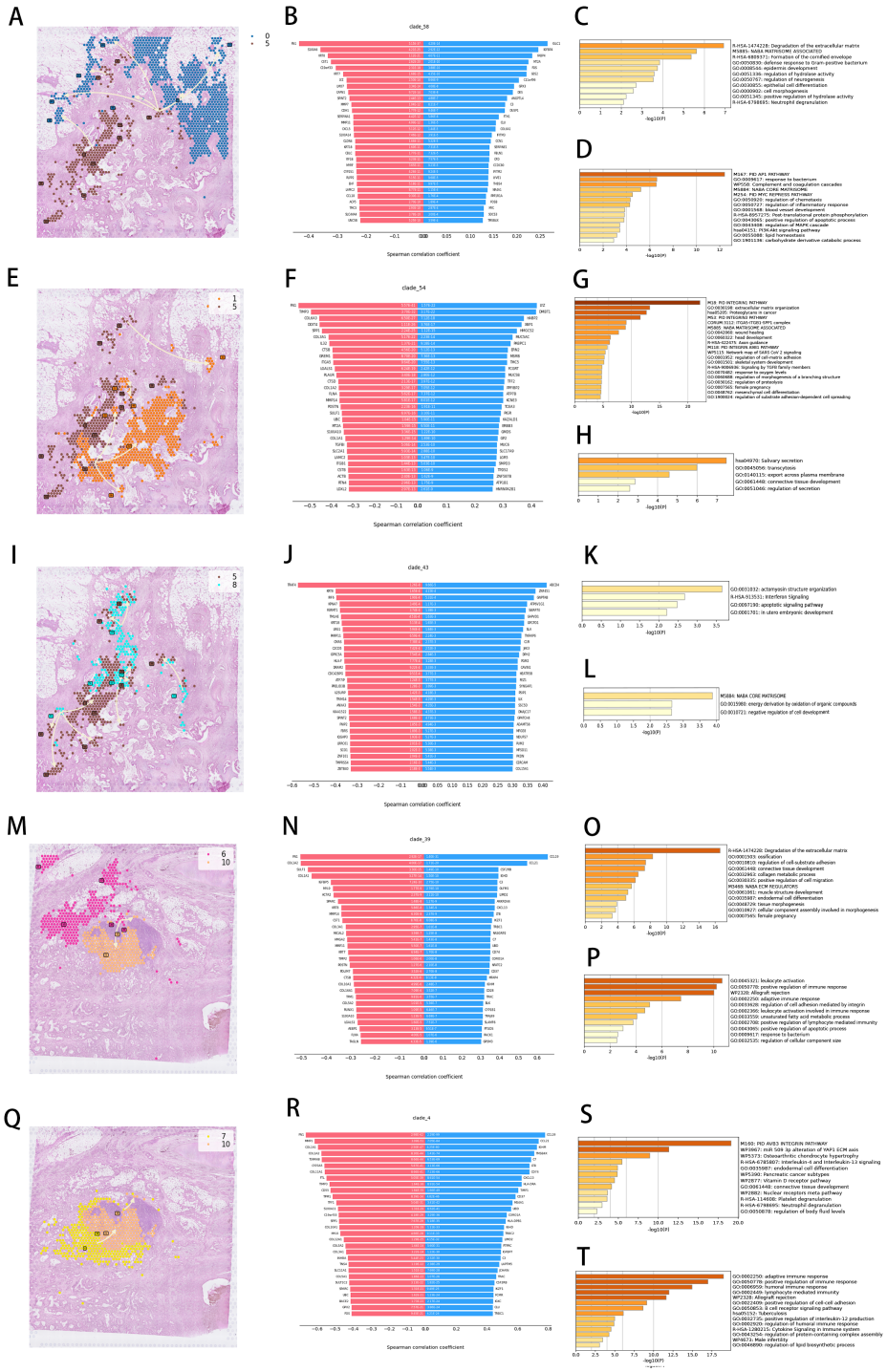

FIGURE 5
Spatial developmental trajectory and enrichment analysis of characteristic genes. **(A, E, I, M, Q)** Developmental trajectory of cell clusters in tissue sections. **(B, F, J, N, R)** Top 30 positively and negatively correlated genes. **(C, G, K, O, S)** Gene enrichment analysis for positively correlated genes. **(D, H, L, P, T)** Gene enrichment analysis for negatively correlated genes.

scaffolding, oxidative stress buffering, and differentiation arrest (Figure 5L).

Cross-cohort validation confirmed conserved temporal logic. Cluster 6→10 progression (Figure 5M) highlighted co-directional activation of ECM proteolysis, FAK signaling, and mesenchymal motility (Figure 5O), contrasted with suppressed leukocyte recruitment and β2-integrin adhesion (Figure 5P). Cluster 7→10 deconvolution (Figure 5Q) demonstrated synchronized αvβ3 integrin mechanosensing, miR-509-3p regulatory hubs, and IL-mediated paracrine signaling (Figure 5S), juxtaposed against attenuated antigen presentation and complement surveillance (Figure 5T).

3.5 Spatial niche specialization of migrasome-enriched fibroblasts and immunomodulatory circuitry

Dynamic spatial profiling of tumor specimens identified fibroblast subpopulations with migrasome accumulation displaying peritumoral localization patterns, coordinating immune-suppressive microenvironment formation through adaptive molecular remodeling. Zonal architecture analysis (Figure 6A) revealed concentric spatial patterning of high-migrasome fibroblasts along tumor-stroma boundaries. Regulatory network decomposition (Figure 6B) delineated counteractive associations between migrasome-enriched fibroblasts and cytotoxic immune cells, particularly demonstrating heightened interface propensity scores for T cell and macrophage populations (Figure 6C). Three-dimensional spatial quantification across distinct anatomical regions – tumor parenchyma (intra), peritumoral stroma (juxta-5μm), and invasive periphery (para-15μm) – (Figure 6D) validated migrasome-rich fibroblast dominance at para-15μm invasion zones.

Core tumor microenvironment evaluation (Figure 6E) revealed operational T cell-epithelial communication networks, implying immune escape mechanisms through direct intercellular signaling. Stromal compartments within juxta-5μm zones (Figure 6F) displayed low-migrasome fibroblast-endothelial assemblies functionally associated with angiogenesis promotion and premetastatic conditioning. Para-15μm invasive territories (Figure 6G) manifested migrasome-dense fibroblast-induced immune silencing, establishing self-contained signaling nodes with diminished leukocyte infiltration.

Multiregional verification analyses (Figures 6H, I) corroborated this spatial architecture, identifying migrasome-enriched fibroblast-mediated immune suppression mechanisms involving STAT3-dependent checkpoint activation and chemokine signaling attenuation. Weighted significance analysis (Figure 6J) coupled with cellular distribution mapping (Figure 6K) enhanced spatial mechanistic interpretation. Intratumoral migrasome-rich fibroblasts (Figure 6L) activated B regulatory pathways via dual IL-10/TGFβ signaling, whereas juxta-5μm low-migrasome counterparts (Figure 6M) facilitated stromal-tumor cooperativity through MMP9/VEGF-A axis activation. Para-15μm migrasome-abundant fibroblasts (Figure 6N) executed L1CAM-integrin mechanical signaling with epithelial cells, potentiating Wnt/β-catenin-mediated proliferative cascades.

3.6 TSPAN4$^+$ fibroblasts as central coordinators in tumor ecosystem networks

Comprehensive multi-platform profiling identified TSPAN4-positive fibroblasts as critical network hubs within tumor microecosystems, exhibiting mutualistic functional partnerships with innate immune components (macrophages, monocytes) and stromal elements (vascular networks). Graph theory-based centrality assessments (Figure 7A) highlighted these fibroblasts as primary conductors of cell-cell communication, whereas boundary signaling evaluations (Figure 7B) characterized their dual role as stromal-immune mediators via selective interactions with endothelial and epithelial interfaces. Reciprocal regulatory axes emerged between adaptive immune clusters, where Th2-skewed T cell/plasma cell interaction metrics (Figure 7C) implied IgE-dependent modulation of antitumor immunity.

Network topology mapping (Figure 7D) delineated TSPAN4$^+$ fibroblasts as core organizers, generating spoke-like connectivity frameworks bridging CD14$^+$ myeloid progenitors, M2-polarized macrophages, and CD31$^+$ vascular units. Spatial interdependency analyses (Figure 7E) uncovered microdomain colocalization patterns between TSPAN4$^+$ fibroblasts and CX3CR1$^+$ monocytic derivatives at tumor invasion zones. Temporal progression modeling (Figure 7F) traced phenotypic diversification trajectories from resting (Cluster 1) to activated fibroblast subtypes (Clusters 4-5), with stepwise TSPAN4 upregulation (Figure 7G) paralleling extracellular matrix remodeling dynamics and SOX9-mediated malignant reprogramming.

3.7 TSPAN4$^+$ fibroblasts as dual regulatory centers in immune-matrix crosstalk

TSPAN4-expressing stromal cells were identified as pivotal regulators of immune suppression and desmoplastic remodeling, operating through multifaceted ligand-receptor (LR) networks involving myeloid (macrophages) and vascular (endothelial) lineages. Spatial colocalization analysis across pancreatic ductal adenocarcinoma microenvironments (Figure 8A) unveiled compartment-specific cellular cooperativity. Systematic LR network mapping (Figure 8B) prioritized high-avidity COL1A2-ITGB1 complexes as key biomechanical signaling units (Figure 8C), with thermodynamic spatial profiling (Figure 8D) highlighting their concentration at stromal-vascular junctions. Directional communication profiling (Figure 8E) revealed asymmetrical signaling dominance from TSPAN4$^+$ fibroblasts to macrophages (via CXCL12-CXCR4 pathways) and endothelial cells (through VEGFC-VEGFR3 cascades).

Graph-based architecture modeling (Figure 8F) established TSPAN4$^+$ fibroblasts as integrative nodes coordinating fibrogenic

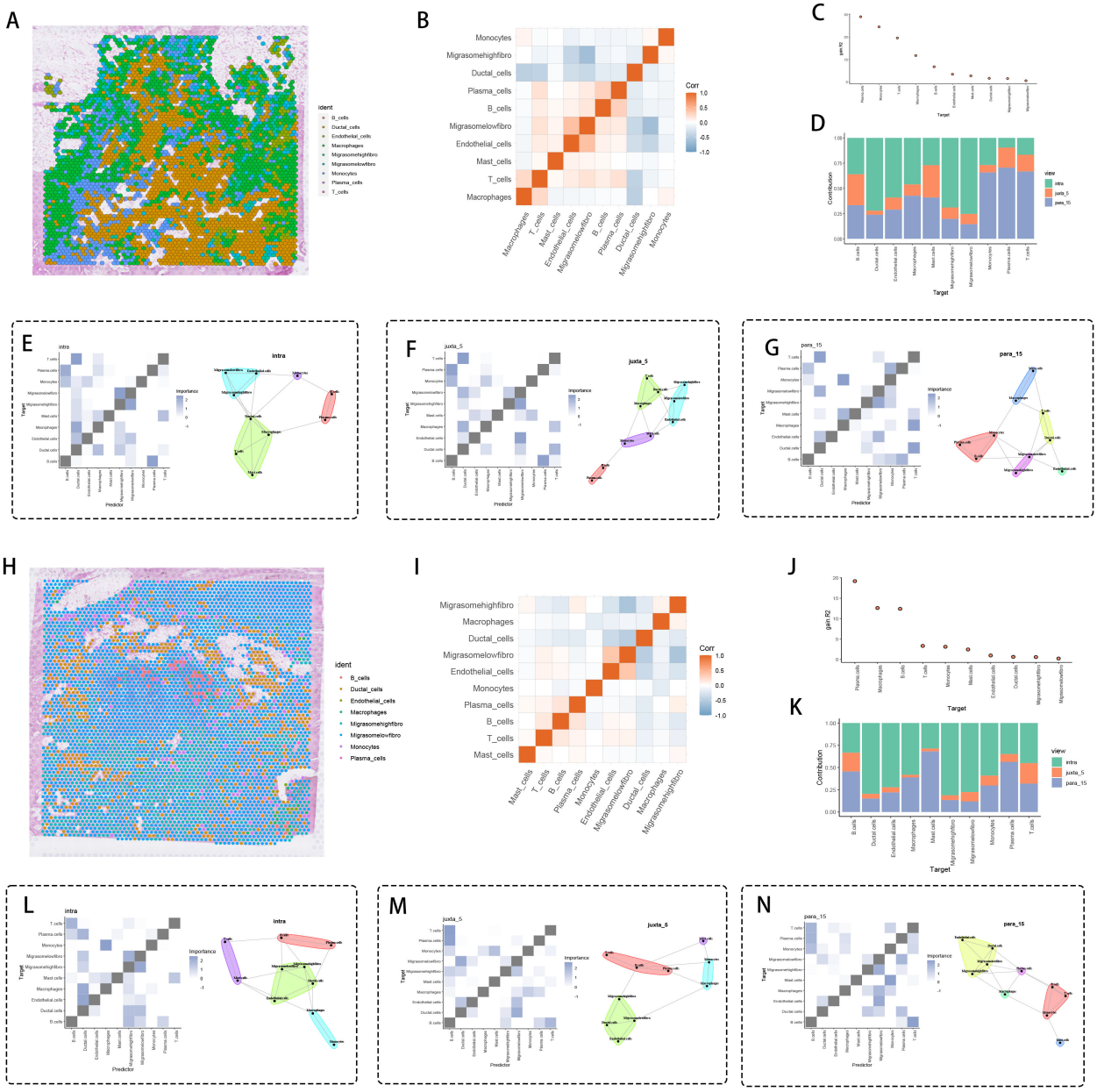

FIGURE 6
Spatial interaction analysis. **(A, H)** Distribution of cell types on tissue sections, with each color representing a different cell type, and migration-related fibroblasts being significantly expressed around cancer tissue. **(B, I)** Correlation heatmap of cell types. **(C, J)** Significance ranking of different cell types. **(D, K)** Bar graph comparing the distribution of different cell types under various conditions (e.g., intra, juxta 5, para 15). Cell interaction networks and significance heatmaps for **(E, L)** para_15, **(F, M)** intra, and **(G, N)** juxta 5 views, showing potential interaction patterns between specific cell types. Spatial zones were defined based on histopathological landmarks: intra-tumoral (within tumor epithelium), juxta-tumoral (≤5 μm from tumor-stroma interface), and para-tumoral (≥15 μm into stroma).

(TGFβ1-LTBP1) and angiogenic (ANGPT2-TIE1) signaling hierarchies. Unified LR pathway mapping (Figure 8G) exposed tri-modal signaling networks linking fibroblast-secreted proteases (MMP2/MMP9) to macrophage phagocytic regulation (CD47-SIRPα) and vascular barrier restructuring (JAM3-ITGAV). Hierarchical network resolution (Figure 8H) characterized TSPAN4$^+$ fibroblasts as stromal control units, harmonizing immune inhibitory (IL10-IL10R) and matrix-condensing (LOXL2-EGFR) mechanisms via spatial orchestration of myeloid and vascular components.

3.8 TSPAN4$^+$ fibroblasts as architects of immunotherapy resistance and checkpoint network configuration

Analysis of the TCGA-PAAD transcriptome identified TSPAN4-positive fibroblasts as critical regulators of immune checkpoint balance. Computational evaluation using the TIDE algorithm (Figure 9A) revealed an inverse relationship between TSPAN4$^+$ fibroblast prevalence and therapeutic efficacy, signifying

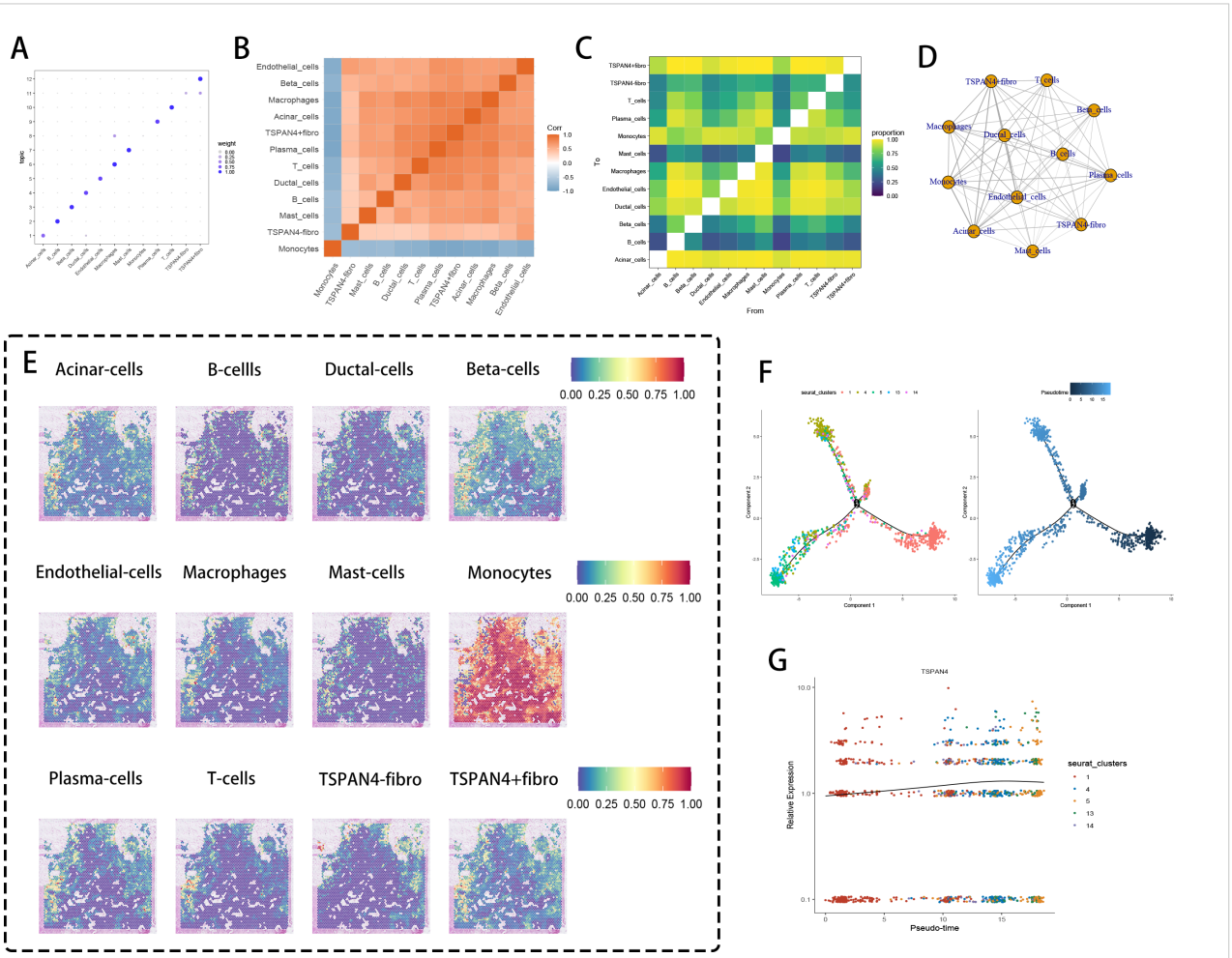

FIGURE 7
Cell cluster interaction and pseudotime analysis. **(A)** Cell cluster correlation weight diagram, where different cell types are weighted in specific themes, with larger bubbles indicating greater importance. **(B)** Correlation heatmap of cell clusters, with red representing positive correlation and blue representing negative correlation. **(C)** Heatmap of cell type interaction ratios, where the color gradient from purple to yellow indicates the strength of interactions (stronger interaction is represented by higher ratios). **(D)** The network topology map showed that TSPAN4+ fibroblasts acted as the core organizer and formed a hub-and-spoke connection framework. **(E)** Distribution of different cell types on tissue sections. **(F, G)** Pseudotime trajectory analysis and TSPAN4 expression in fibroblast subgroups.

stroma-driven immune suppression. Multidimensional covariance analysis (Figure 9B) uncovered synchronized transcriptional patterns linking these fibroblasts to $CD8^+$ T cell dysfunction ($p=7.51\times10^{-6}$), with lineage specification profiling (Figure 9C) confirming their canonical stromal origin ($p=1.96\times10^{-37}$). Energy-based correlation networks (Figure 9D) mapped TSPAN4's functional integration with immune escape components (CD27, CTLA4, PDCD1, TNFRSF; r=0.5–0.9), further substantiated by dual-axis interaction analysis (Figure 9E) demonstrating concurrent associations with both activating (CD28) and suppressive (TIM3) immune receptors.

Regulatory network topology (Figure 9F) characterized TSPAN4's transcriptional interplay with matrix regulators (TYRBP9, TSPAN9) and stromal adaptability markers (VIM, VASN). Immune compartment decoding (Figure 9G) revealed counterintuitive relationships: robust $FOXP3^+$ regulatory T cell ($p=0.003$) and immature B cell recruitment contrasted with diminished antigen-presenting cell interactions. Transcriptional covariance networks (Figure 9H) further confirmed TSPAN4's integration with protein homeostasis (UBTQ1) and mesenchymal transition (WTIP) pathways. Notably, TSPAN4 displayed inverse correlation with genomic instability (R=-0.16, p=0.046) (Figure 9I), implying its involvement in shaping immunologically silent microenvironments via tumor mutational burden regulation.

3.9 TSPAN4 knockdown suppresses malignant progression in pancreatic cancer models

Gene-specific suppression of TSPAN4 was confirmed through quantitative polymerase chain reaction (qPCR), with siRNA-mediated silencing achieving substantial mRNA downregulation in SW1990 ($p < 0.001$) and PANC-1 ($p < 0.0001$) cell lines relative to scramble controls (Figure 10A). Functional characterization uncovered potent growth-inhibitory effects, as evidenced by CCK-8 proliferation assays

10.3389/fimmu.2025.1594879

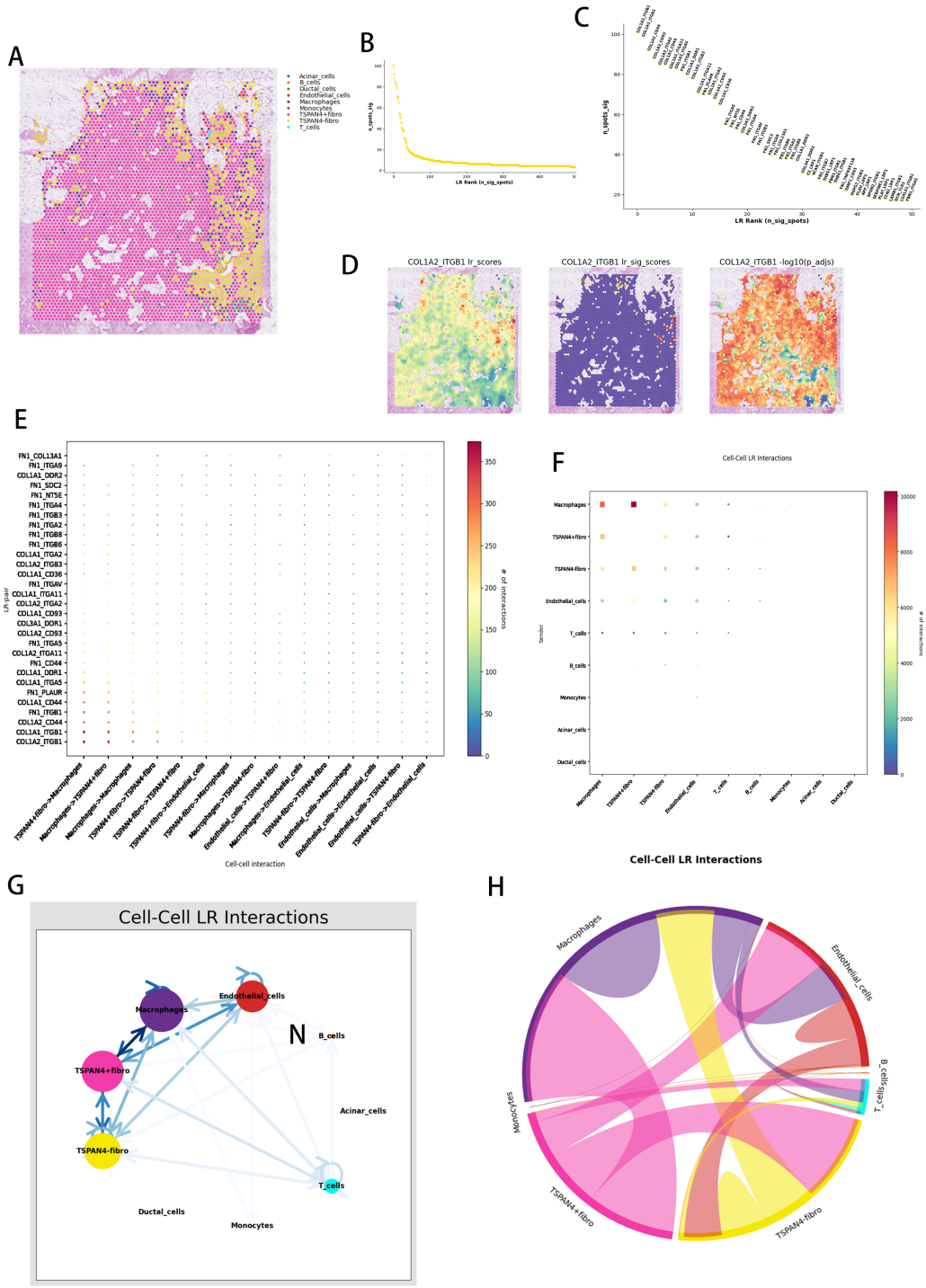

FIGURE 8
Spatial ligand-receptor pair interaction analysis. **(A)** Spatial distribution of cell types within tissue sections, with different colors representing various cell types. **(B)** Ligand-receptor (LR) score distribution. **(C)** Ranking of ligand-receptor pairs based on significance. **(D)** Spatial distribution of the COL1A2_ITGB1 ligand-receptor pair. **(E)** Cell-to-cell ligand-receptor (LR) interaction point diagram, where each point represents a ligand-receptor pair, and the color indicates the number of interactions (from blue for low interaction to red for high interaction). **(F)** Overall cell-to-cell ligand-receptor interaction network. **(G)** Ligand-receptor interaction networks between various cell types, with color intensity reflecting interaction strength. **(H)** Cell-to-cell interaction signaling pathway network chord diagram.

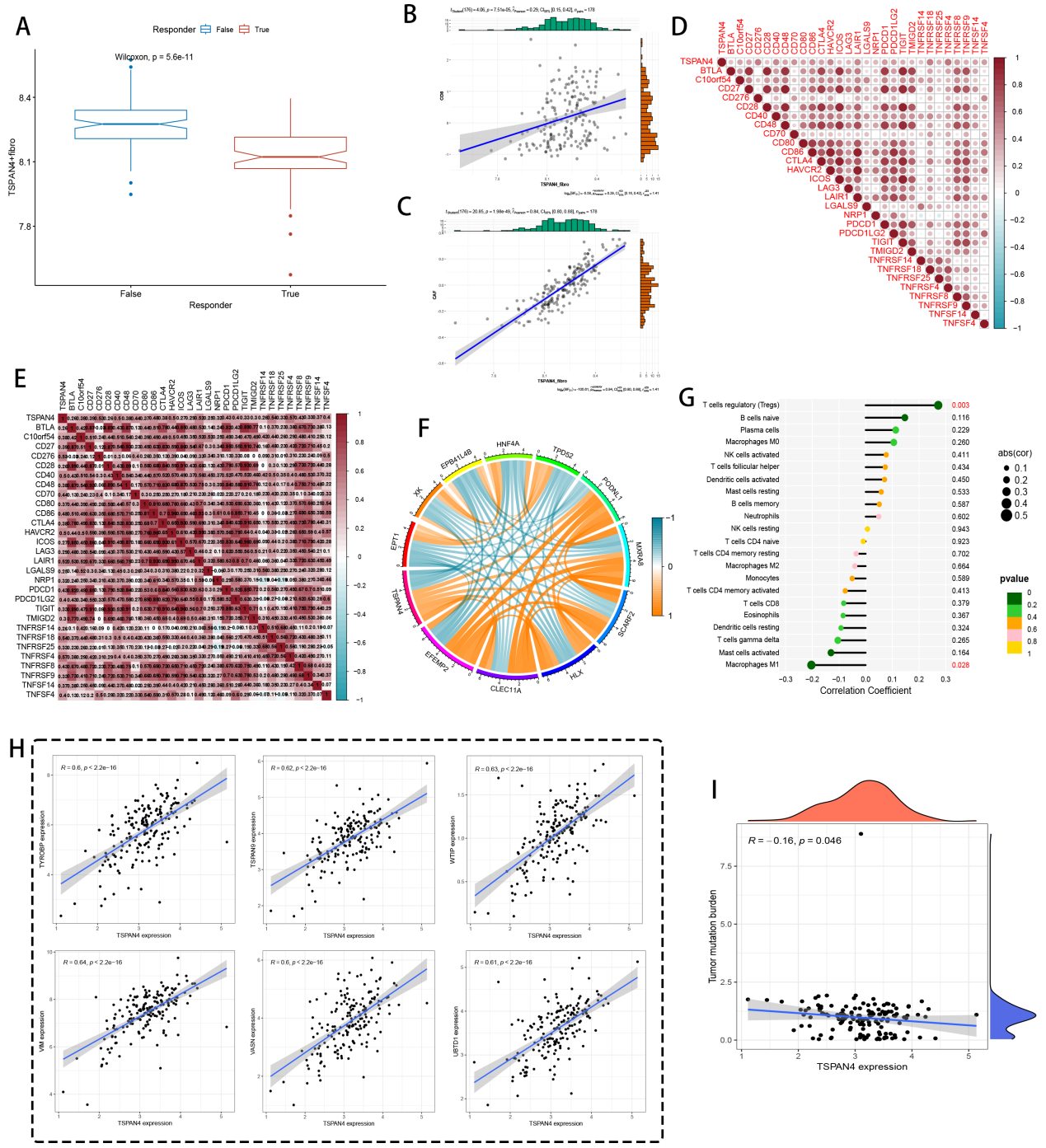

FIGURE 9
Immune therapy and immune microenvironment analysis at the bulk level. **(A)** TIDE immune therapy boxplot, with a Wilcoxon test p-value of 5.6e-11, indicating statistical significance. **(B, C)** Correlation analysis between TSPAN4+ fibroblasts and immune-related markers. **(D)** Heatmap showing the correlation of TSPAN4 with immune checkpoint and inflammatory marker genes, with red representing positive correlation and blue representing negative correlation. **(E)** Heatmap of TSPAN4 correlation with other immune marker genes. **(F)** Chord diagram displaying gene relationships and co-expression, with color indicating correlation strength (blue for negative correlation, orange for positive correlation). **(G)** Bar graph showing the correlation between TSPAN4 expression and various immune cell subpopulations (e.g., regulatory T cells, B cells). **(H)** Scatter plot showing the correlation between TSPAN4 expression and various gene expressions. **(I)** Heatmap of TSPAN4 expression correlated with tumor mutation burden.

showing progressive suppression of cellular viability over a 96-hour observation period (SW1990: $p < 0.01$; PANC-1: $p < 0.001$) (Figure 10B). Colony formation analyses further validated these observations, revealing near-total elimination of clonogenic capacity in both models (SW1990: $p < 0.0001$; PANC-1: $p < 0.001$), consistent with disrupted tumorigenic self-renewal mechanisms (Figure 10C). In parallel assessments of metastatic behavior, TSPAN4-depleted cells exhibited statistically significant migratory impairment at 48 hours post-transfection, demonstrating 82% invasion reduction in SW1990 ($p < 0.0001$) and 63% attenuation in PANC-1 ($p < 0.05$), thereby establishing TSPAN4's functional necessity for metastatic competence (Figure 10D).

3.10 TSPAN4 knockdown inhibits metastatic potential and triggers apoptotic activation

Genetic silencing of TSPAN4 significantly impaired invasive behavior in pancreatic cancer cell models (SW1990/PANC-1). Quantitative assessment of cellular invasion demonstrated 4.7-fold (SW1990: $p < 0.0001$) and 3.9-fold (PANC-1: $p < 0.0001$) suppression of transmigration capacity, establishing TSPAN4's mechanistic involvement in preparing metastatic microenvironments (Figure 11A). Cytometric analysis uncovered apoptosis-promoting reprogramming, with TSPAN4-depleted cells showing dramatic increases in programmed cell death: SW1990 apoptotic rates surged from 0.08% (control) to 11.56% ($p < 0.001$), while PANC-1 apoptosis rose from 2.09% to 12.87% ($p < 0.01$), confirming caspase-mediated death pathway activation (Figure 11B).

4 Discussion

Pancreatic cancer is a highly malignant tumor originating from the pancreas, often presenting asymptomatically in its early stages (44, 45). This lack of symptoms contributes to delayed diagnosis and poor prognosis (46). Treatment remains particularly challenging due to the absence of early-stage markers and the deep location of the pancreas within the abdomen, which complicates detection during routine examinations (47–49). While surgical resection can improve patient survival, the overall survival rate remains dismal because most patients are diagnosed at advanced stages. Thus, early screening and diagnosis are critical to improving survival outcomes (50–52).

Migrasomes, which are membrane-bound structures formed during cell migration, are typically composed of cytoplasmic vesicles or inclusions (53). These structures play crucial roles in signal transduction, matrix remodeling, and facilitating cell movement by altering cell membrane morphology and aiding material transport (54), and it plays an important role in intercellular communication (55). Migrasomes are integral to overcoming physical barriers and enhancing cell motility, enabling tumor cells to navigate the ECM and migrate to distant sites (56). Furthermore, migrasomes have been shown to regulate the organization of microtubules and microfilaments, influencing the shape and motility of tumor cells and contributing to metastasis by facilitating the movement of tumor cells into the bloodstream or lymphatic system (54). While migrasomes are recognized as metastasis facilitators (57), their role in fibroblast-immune crosstalk remains contentious. Our work resolves this by demonstrating context-dependent migrasome functions, contingent on fibroblast-TSPAN4 expression. Among them, TSPAN4 has been confirmed to be associated with the prognosis of a variety of cancers (58, 59).

In the present study, it was observed that fibroblasts derived from metastatic and primary pancreatic cancer tissues exhibited a notable upregulation of genes associated with migration, including TSPAN4 and ITGA5. These observations are in alignment with earlier research that has demonstrated the pivotal role of fibroblasts in facilitating tumor cell migration, invasion, and metastasis through their interactions within the tumor microenvironment (60–62). The observation of significant signaling between fibroblasts expressing high levels of migrator-related genes and other cell types, including macrophages, endothelial cells, and ductal cells, suggests that fibroblasts interact with immune cells and stromal components to collectively regulate the tumor microenvironment (63–65). Of particular interest, we found through enrichment analysis that signaling pathways such as PERIOSTIN, FGF and ANGPTL were highly enriched in Migrasomehighfibro cells, suggesting that these fibroblasts may affect cancer cell migration and invasion through mechanisms such as the PI3K/Akt pathway (50, 66). This synergistic cellular environment may drive pancreatic cancer progression, particularly in terms of ECM remodeling and immune evasion (67).

The correlation of TSPAN4 expression with immune checkpoint markers such as PDCD1 and CTLA4 further suggests that $TSPAN4^+$ fibroblasts may reduce the effectiveness of immunotherapy (68). Indeed, patients exhibiting high expression of $TSPAN4^+$ fibroblasts displayed poorer responses to immunotherapy, highlighting the potential of TSPAN4 as both a prognostic marker and a therapeutic target (69).

Tetraspanin 4 (TSPAN4), a member of the transmembrane 4 superfamily, has emerged as a potential contributor to the pathogenesis of pancreatic cancer. The broader TSPAN family has been implicated in multiple oncogenic processes in this malignancy. For instance, TSPAN1 has been shown to promote autophagy via the MIR454–FAM83A–TSPAN1 regulatory axis and facilitates the crosstalk between WNT–CTNNB1 signaling and autophagic pathways in pancreatic cancer (70). Notably, the extracellular domain of TSPAN4 offers a viable target for monoclonal antibody-based therapies, in line with ongoing efforts to develop TSPAN-directed therapeutics (71). Furthermore, gene-editing technologies such as CRISPR/Cas9, or the application of small-molecule inhibitors to disrupt TSPAN4–integrin interactions, may enhance the efficacy of current immunotherapies by overcoming resistance mechanisms and modifying the tumor immune microenvironment (72).

Further studies found that fibroblasts with high expression of migrator-related genes interact weakly with immune cells such as T cells and macrophages, suggesting that they may play an

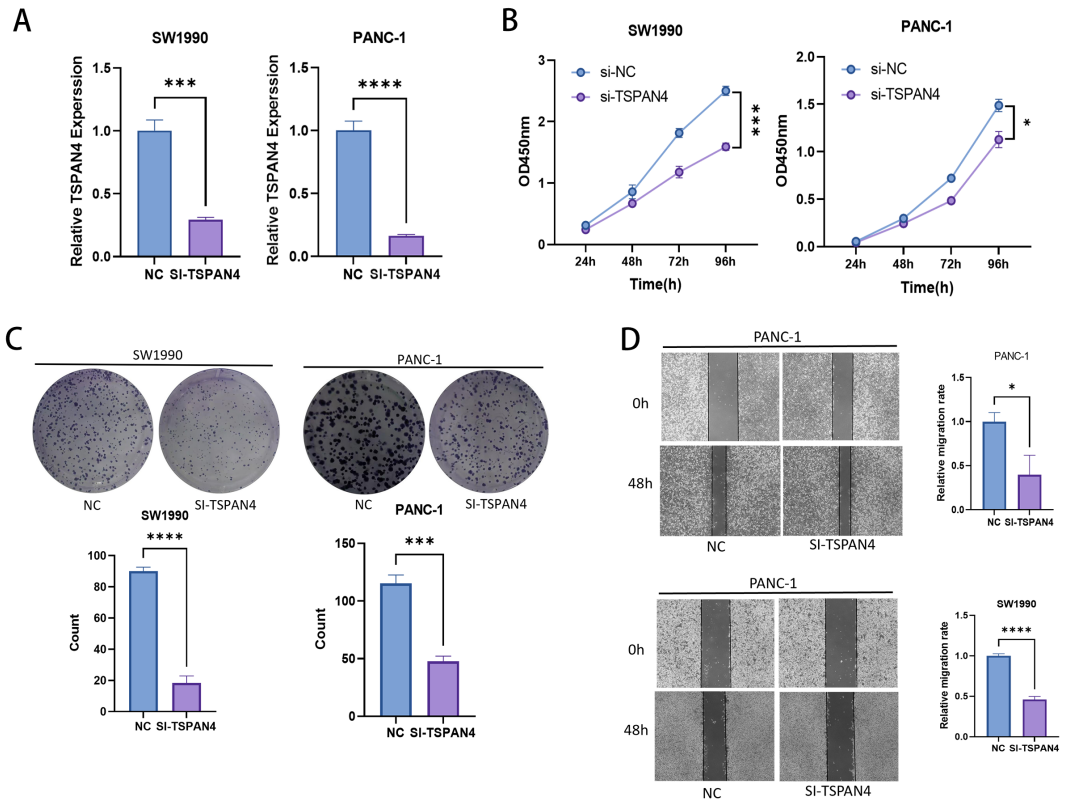

FIGURE 10
Cell experiments. **(A)** PCR histograms and **(B)** CCK-8 cell proliferation assay line plots for normal and TSPAN4 low-expression groups in SW1990 and PANC-1 cell lines. **(C)** Microscopic images and histogram results from the clone formation assay in SW1990 and PANC-1 cells. **(D)** Microscopic images and histogram results of the wound healing assay. *: p<0.05; **: p<0.01; ***: p<0.001; ****p<0.0001.

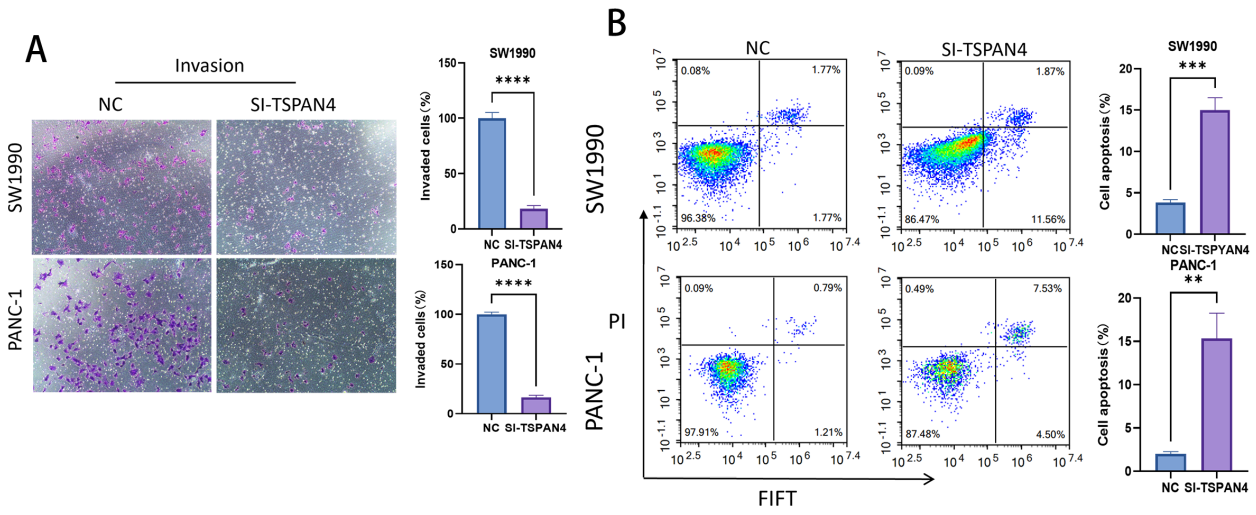

FIGURE 11
Cell experiments. **(A)** Microscopic images and histogram analysis of Transwell invasion assays, showing the invasion ability of SW1990 and PANC-1 cells after TSPAN4 knockdown compared to the control group. **(B)** Flow cytometry dot plots and histogram analysis showing apoptosis rates of SW1990 and PANC-1 cells after TSPAN4 knockdown. *: p<0.05; **: p<0.01; ***: p<0.001; ****p<0.0001.

immunosuppressive role in the tumor microenvironment (73). Interestingly, TSPAN4$^+$ fibroblasts were significantly more in the responder group than in the non-responder group and showed strong positive correlations with multiple immune cell interactions. This phenomenon highlights that TSPAN4$^+$ fibroblasts contribute to tumor immune escape and progression.

Single-cell resolution mitigated tumor heterogeneity biases, yet spatial variability warrants further exploration. Spatial transcriptomic analysis revealed significant spatial heterogeneity in the expression of migrator-related genes in different cell populations of pancreatic cancer (74). The complex distribution of TSPAN4 and ITGA5 likely with pancreatic cancer cell migration, proliferation, and ECM degradation highlights the dynamic interactions between cells that drive pancreatic cancer metastasis.

In the TSPAN4 knockdown assay, knockdown of TSPAN4 significantly reduced the proliferation and migration ability of SW1990 and PANC-1 cells, suggesting that TSPAN4 promotes tumor malignancy by promoting cancer cell migration and invasion.

While TSPAN4 emerged as a focal regulator, ITGA5 also demonstrated pan-stromal expression, suggesting complementary roles in ECM adhesion and integrin-mediated mechanotransduction (75). Future studies should dissect ITGA5's distinct contributions to migrasome signaling and stromal crosstalk.

However, although our study still has some limitations such as the single cell dataset only included 3 clinical cohorts (2 primary cancers, 2 metastatic cancers, and 1 normal tissue), and the detailed molecular mechanism of TSPAN4 in inducing fibroblasts to promote pancreatic cancer progression needs to be further investigated.

Furthermore, the development of therapeutic strategies targeting TSPAN4 may block tumor progression and metastasis and enhance the efficacy of existing immunotherapies. In-depth study of the specific mechanisms by which TSPAN4$^+$ fibroblasts regulate immune responses and extracellular matrix remodeling using spatial transcriptomics will be essential for the development of targeted therapeutic strategies against pancreatic cancer (76).

5 Conclusion

Utilizing single-cell RNA sequencing and spatial transcriptomics, this study identified migrator-associated genes, including *TSPAN4* and *ITGA5*, as critical regulators of fibroblast function in pancreatic cancer. Notably, *TSPAN4*$^+$ fibroblasts were found to play pivotal roles in shaping the tumor microenvironment by promoting tumor progression, metastasis, immune evasion, and ECM remodeling. These findings highlight the potential of *TSPAN4*$^+$ fibroblasts as therapeutic targets and provide novel insights into the stromal dynamics driving pancreatic cancer malignancy.

Data availability statement

The original contributions presented in the study are included in the article/supplementary material. Further inquiries can be directed to the corresponding authors.

Ethics statement

Ethical approval was not required for the studies on humans in accordance with the local legislation and institutional requirements because only commercially available established cell lines were used.

Author contributions

QH: Writing – original draft, Formal analysis, Visualization, Data curation, Conceptualization. JC: Writing – original draft, Conceptualization. YL: Writing – original draft, Conceptualization. HC: Visualization, Formal analysis, Data curation, Writing – original draft. HL: Visualization, Formal analysis, Writing – original draft, Data curation. LJ: Data curation, Formal analysis, Writing – original draft, Visualization. XCZ: Visualization, Formal analysis, Data curation, Writing – original draft. SZ: Writing – original draft, Formal analysis, Data curation. JH: Data curation, Writing – original draft, Formal analysis. HC: Conceptualization, Writing – review & editing. BL: Writing – review & editing, Conceptualization. XLZ: Conceptualization, Writing – review & editing.

Funding

The author(s) declare that financial support was received for the research and/or publication of this article. The study was approved by Sichuan Medical Science and Technology Innovation Research Association (SCMSIA) Launches "Top of Medical Innovation" Specialized Research Project (No.YCH-KY-YCZD2024-298) and Southwest Medical University 2024 innovative training program for college students (S202410632176).

Acknowledgments

We gratefully acknowledge the Gene Expression Omnibus (GEO), The Cancer Genome Atlas (TCGA), International Cancer Genome Consortium(ICGC),and the UCSC Xena website for their public datasets. We also appreciate the R programming language community for the essential tools that facilitated our research.

Conflict of interest

The authors hereby declare that there were no commercial or financial relationships that could be interpreted as potential conflicts of interest in this study.

Generative AI statement

The author(s) declare that Generative AI was used in the creation of this manuscript.

The use of generative artificial intelligence tools (such as ChatGPT, etc.) in the writing process of this study was limited to the following auxiliary work: language polishing and readability optimization, sentence adjustment, terminology normalization and expression fluency improvement of English text; Non-professional expressions are simplified, and complex academic expressions are transformed into texts that are more in line with the reading habits of journal readers. It is important to note that all changes made by generative AI were manually reviewed sentence by sentence by the authors to ensure that they did not change the scientific meaning of the original data. AI was not allowed to participate in core academic content such as study design, data analysis, conclusion derivation, and chart/formula creation. Despite the use of AI-assisted language, the authors are solely responsible for all views, data, and results presented in the manuscript.

Publisher's note

References

1. Li T, Wang Z, Hou YF, Li YY. Pim-3 regulates stemness of pancreatic cancer cells via activating STAT3 signaling pathway. *J Cancer*. (2017) 8:1530–41. doi: 10.7150/jca.18628

2. Jiang L, Liu J, Zhang S, Jiang C, Huang J, Chen H, et al. Role of glycosylation-related gene MGAT1 in pancreatic ductal adenocarcinoma. *Front Immunol*. (2024) 15:1438935. doi: 10.3389/fimmu.2024.1438935

3. Kommalapati A, Tella SH, Goyal G, Ma WW, Mahipal A. Contemporary management of localized resectable pancreatic cancer. *Cancers*. (2018) 10:24. doi: 10.3390/cancers10010024

4. Liu L, Xie Y, Yang H, Lin A, Dong M, Wang H, et al. HPVTIMER: A shiny web application for tumor immune estimation in human papillomavirus-associated cancers. *iMeta*. (2023) 2:e130. doi: 10.1002/imt2.v2.3

5. Shi X, Cheng X, Jiang A, Shi W, Zhu L, Mou W, et al. Immune checkpoints in B cells: unlocking new potentials in cancer treatment. *Advanced Sci (Weinheim Baden-Wurttemberg Germany)*. (2024) 11:e2403423. doi: 10.1002/advs.202403423

6. Hirakawa T, Yashiro M, Murata A, Hirata K, Kimura K, Amano R, et al. IGF-1 receptor and IGF binding protein-3 might predict prognosis of patients with resectable pancreatic cancer. *BMC cancer*. (2013) 13:392. doi: 10.1186/1471-2407-13-392

7. Chan R, Sethi P, Jyoti A, McGarry R, Upreti M. Investigating the radioresistant properties of lung cancer stem cells in the context of the tumor microenvironment. *Radiat Res*. (2016) 185:169–81. doi: 10.1667/RR14285.1

8. Kawase T, Yasui Y, Nishina S, Hara Y, Yanatori I, Tomiyama Y, et al. Fibroblast activation protein-α-expressing fibroblasts promote the progression of pancreatic ductal adenocarcinoma. *BMC gastroenterology*. (2015) 15:109. doi: 10.1186/s12876-015-0340-0

9. Agnoletto C, Pignochino Y, Caruso C, Garofalo C. Exosome-based liquid biopsy approaches in bone and soft tissue sarcomas: review of the literature, prospectives, and hopes for clinical application. *Int J Mol Sci*. (2023) 24:5159. doi: 10.3390/ijms24065159

10. Wu H, Zhu X, Zhou H, Sha M, Ye J, Yu H. Mitochondrial ribosomal proteins and cancer. *Medicina (Kaunas Lithuania)*. (2025) 61:96. doi: 10.3390/medicina61010096

11. Jiang D, Jiang Z, Lu D, Wang X, Liang H, Zhang J, et al. Migrasomes provide regional cues for organ morphogenesis during zebrafish gastrulation. *Nat Cell Biol*. (2019) 21:966–77. doi: 10.1038/s41556-019-0358-6

12. Jiang Y, Liu X, Ye J, Ma Y, Mao J, Feng D, et al. Migrasomes, a new mode of intercellular communication. *Cell communication signaling: CCS*. (2023) 21:105. doi: 10.1186/s12964-023-01121-4

13. Zheng Y, Lang Y, Qi B, Li T. TSPAN4 and migrasomes in atherosclerosis regression correlated to myocardial infarction and pan-cancer progression. *Cell adhesion migration*. (2023) 17:14–9. doi: 10.1080/19336918.2022.2155337

14. Qin Y, Yang J, Liang C, Liu J, Deng Z, Yan B, et al. Pan-cancer analysis identifies migrasome-related genes as a potential immunotherapeutic target: A bulk omics research and single cell sequencing validation. *Front Immunol*. (2022) 13:994828. doi: 10.3389/fimmu.2022.994828

15. Lin S, Li D, Yang Y, Yu M, Zhao R, Li J, et al. Single-cell RNA-seq elucidates the crosstalk between cancer stem cells and the tumor microenvironment in hepatocellular carcinoma. *J Cancer*. (2024) 15:1093–109. doi: 10.7150/jca.92185

16. Panebianco C, Ciardiello D, Villani A, Maiorano BA, Latiano TP, Maiello E, et al. Insights into the role of gut and intratumor microbiota in pancreatic ductal adenocarcinoma as new key players in preventive, diagnostic and therapeutic perspective. *Semin Cancer Biol*. (2022) 86:997–1007. doi: 10.1016/j.semcancer.2021.11.007

17. Ritchie ME, Phipson B, Wu D, Hu Y, Law CW, Shi W, et al. limma powers differential expression analyses for RNA-sequencing and microarray studies. *Nucleic Acids Res*. (2015) 43:e47. doi: 10.1093/nar/gkv007

18. Chu C, Lin EW, Tran A, Jin H, Ho NI, Veit A, et al. The landscape of human SVA retrotransposons. *Nucleic Acids Res*. (2023) 51:11453–65. doi: 10.1093/nar/gkad821

19. Butler A, Hoffman P, Smibert P, Papalexi E, Satija R. Integrating single-cell transcriptomic data across different conditions, technologies, and species. *Nat Biotechnol*. (2018) 36:411–20. doi: 10.1038/nbt.4096

20. Marco Salas S, Gyllborg D, Mattsson Langseth C, Nilsson M. Matisse: a MATLAB-based analysis toolbox for in *situ* sequencing expression maps. *BMC Bioinf*. (2021) 22:391. doi: 10.1186/s12859-021-04302-5

21. Hochbaum DR, Hulshof L, Urke A, Wang W, Dubinsky AC, Farnsworth HC, et al. Thyroid hormone remodels cortex to coordinate body-wide metabolism and exploration. *Cell*. (2024) 187:5679–97.e23. doi: 10.1016/j.cell.2024.07.041

22. Fan C, Chen F, Chen Y, Huang L, Wang M, Liu Y, et al. irGSEA: the integration of single-cell rank-based gene set enrichment analysis. *Briefings Bioinf*. (2024) 25:243. doi: 10.1093/bib/bbae243

23. Trapnell C, Cacchiarelli D, Grimsby J, Pokharel P, Li S, Morse M, et al. The dynamics and regulators of cell fate decisions are revealed by pseudotemporal ordering of single cells. *Nat Biotechnol*. (2014) 32:381–6. doi: 10.1038/nbt.2859

24. Qiu X, Hill A, Packer J, Lin D, Ma YA, Trapnell C. Single-cell mRNA quantification and differential analysis with Census. *Nat Methods*. (2017) 14:309–15. doi: 10.1038/nmeth.4150

25. Qiu X, Mao Q, Tang Y, Wang L, Chawla R, Pliner HA, et al. Reversed graph embedding resolves complex single-cell trajectories. *Nat Methods*. (2017) 14:979–82. doi: 10.1038/nmeth.4402

26. Korsunsky I, Millard N, Fan J, Slowikowski K, Zhang F, Wei K, et al. Fast, sensitive and accurate integration of single-cell data with Harmony. *Nat Methods*. (2019) 16:1289–96. doi: 10.1038/s41592-019-0619-0

27. Macnair W, Gupta R, Claassen M. psupertime: supervised pseudotime analysis for time-series single-cell RNA-seq data. *Bioinf (Oxford England)*. (2022) 38:i290–i8. doi: 10.1093/bioinformatics/btac227

28. Wolf FA, Angerer P, Theis FJ. SCANPY: large-scale single-cell gene expression data analysis. *Genome Biol*. (2018) 19:15. doi: 10.1186/s13059-017-1382-0

29. Jiang X, Dong L, Wang S, Wen Z, Chen M, Xu L, et al. Reconstructing spatial transcriptomics at the single-cell resolution with bayesDeep. *bioRxiv: preprint server Biol*. (2023). doi: 10.1101/2023.12.07.570715

30. Zhang Y, Liu T, Hu X, Wang M, Wang J, Zou B, et al. CellCall: integrating paired ligand-receptor and transcription factor activities for cell-cell communication. *Nucleic Acids Res*. (2021) 49:8520–34. doi: 10.1093/nar/gkab638

31. Jin S, Guerrero-Juarez CF, Zhang L, Chang I, Ramos R, Kuan CH, et al. Inference and analysis of cell-cell communication using CellChat. *Nat communications*. (2021) 12:1088. doi: 10.1038/s41467-021-21246-9

32. Hafemeister C, Satija R. Normalization and variance stabilization of single-cell RNA-seq data using regularized negative binomial regression. *Genome Biol*. (2019) 20:296. doi: 10.1186/s13059-019-1874-1

33. Yang H, Chen CB, Kumara S. Heterogeneous recurrence analysis of spatial data. *Chaos (Woodbury NY)*. (2020) 30:013119. doi: 10.1063/1.5129959

34. Wu Y, Yang S, Ma J, Chen Z, Song G, Rao D, et al. Spatiotemporal immune landscape of colorectal cancer liver metastasis at single-cell level. *Cancer discovery*. (2022) 12:134–53. doi: 10.1158/2159-8290.CD-21-0316

35. Martínez VS, Saa PA, Jooste J, Tiwari K, Quek LE, Nielsen LK. The topology of genome-scale metabolic reconstructions unravels independent modules and high network flexibility. *PloS Comput Biol*. (2022) 18:e1010203. doi: 10.1371/journal.pcbi.1010203

36. Chen H, Zuo H, Huang J, Liu J, Jiang L, Jiang C, et al. Unravelling infiltrating T-cell heterogeneity in kidney renal clear cell carcinoma: Integrative single-cell and spatial transcriptomic profiling. *J Cell Mol medicine*. (2024) 28:e18403. doi: 10.1111/jcmm.v28.12

37. Huan C, Li J, Li Y, Zhao S, Yang Q, Zhang Z, et al. Spatially resolved multiomics: data analysis from monoomics to multiomics. *BME frontiers*. (2025) 6:0084. doi: 10.34133/bmef.0084

38. Zhou Y, Zhou B, Pache L, Chang M, Khodabakhshi AH, Tanaseichuk O, et al. Metascape provides a biologist-oriented resource for the analysis of systems-level datasets. *Nat communications*. (2019) 10:1523. doi: 10.1038/s41467-019-09234-6

39. Tu H, Hu Q, Ma Y, Huang J, Luo H, Jiang L, et al. Deciphering the tumour microenvironment of clear cell renal cell carcinoma: Prognostic insights from programmed death genes using machine learning. *J Cell Mol medicine*. (2024) 28: e18524. doi: 10.1111/jcmm.v28.13

40. Tanevski J, Flores ROR, Gabor A, Schapiro D, Saez-Rodriguez J. Explainable multiview framework for dissecting spatial relationships from highly multiplexed data. *Genome Biol*. (2022) 23:97. doi: 10.1186/s13059-022-02663-5

41. Cable DM, Murray E, Zou LS, Goeva A, Macosko EZ, Chen F, et al. Robust decomposition of cell type mixtures in spatial transcriptomics. *Nat Biotechnol*. (2022) 40:517–26. doi: 10.1038/s41587-021-00830-w

42. Elosua-Bayes M, Nieto P, Mereu E, Gut I, Heyn H. SPOTlight: seeded NMF regression to deconvolute spatial transcriptomics spots with single-cell transcriptomes. *Nucleic Acids Res*. (2021) 49:e50. doi: 10.1093/nar/gkab043

43. Hänzelmann S, Castelo R, Guinney J. GSVA: gene set variation analysis for microarray and RNA-seq data. *BMC Bioinf*. (2013) 14:7. doi: 10.1186/1471-2105-14-7

44. Tian Z, Liang G, Cui K, Liang Y, Wang Q, Lv S, et al. Insight into the prospects for RNAi therapy of cancer. *Front Pharmacol*. (2021) 12:644718. doi: 10.3389/fphar.2021.644718

45. Chi H, Su L, Yan Y, Gu X, Su K, Li H, et al. Illuminating the immunological landscape: mitochondrial gene defects in pancreatic cancer through a multiomics lens. *Front Immunol*. (2024) 15:1375143. doi: 10.3389/fimmu.2024.1375143

46. Bray F, Ferlay J, Soerjomataram I, Siegel RL, Torre LA, Jemal A. Global cancer statistics 2018: GLOBOCAN estimates of incidence and mortality worldwide for 36 cancers in 185 countries. *CA: A Cancer J clinicians*. (2018) 68:394–424. doi: 10.3322/caac.21492

47. Ideno N, Mori Y, Nakamura M, Ohtsuka T. Early detection of pancreatic cancer: role of biomarkers in pancreatic fluid samples. *Diagnostics (Basel Switzerland)*. (2020) 10:1056. doi: 10.3390/diagnostics10121056

48. Amaral MJ, Oliveira RC, Donato P, Tralhão JG. Pancreatic cancer biomarkers: oncogenic mutations, tissue and liquid biopsies, and radiomics-A review. *Digestive Dis Sci*. (2023) 68:2811–23. doi: 10.1007/s10620-023-07904-6

49. Chi H, Peng G, Wang R, Yang F, Xie X, Zhang J, et al. Cuprotosis programmed-cell-death-related lncRNA signature predicts prognosis and immune landscape in PAAD patients. *Cells*. (2022) 11:3436. doi: 10.3390/cells11213436

50. Man Q, Pang H, Liang Y, Chang S, Wang J, Gao S. Nomogram model for predicting early recurrence for resectable pancreatic cancer: A multicenter study. *Medicine*. (2024) 103:e37440. doi: 10.1097/MD.0000000000037440

51. Spiers L, Gray M, Lyon P, Sivakumar S, Bekkali N, Scott S, et al. Clinical trial protocol for PanDox: a phase I study of targeted chemotherapy delivery to non-resectable primary pancreatic tumours using thermosensitive liposomal doxorubicin (ThermoDox®) and focused ultrasound. *BMC cancer*. (2023) 23:896. doi: 10.1186/s12885-023-11228-z

52. Huang X, Chi H, Gou S, Guo X, Li L, Peng G, et al. An aggrephagy-related lncRNA signature for the prognosis of pancreatic adenocarcinoma. *Genes*. (2023) 14:124. doi: 10.3390/genes14010124

53. Huang Y, Zucker B, Zhang S, Elias S, Zhu Y, Chen H, et al. Publisher Correction: Migrasome formation is mediated by assembly of micron-scale tetraspanin macrodomains. *Nat Cell Biol*. (2019) 21:1301. doi: 10.1038/s41556-019-0389-z

54. Zhang K, Zhu Z, Jia R, Wang NA, Shi M, Wang Y, et al. CD151-enriched migrasomes mediate hepatocellular carcinoma invasion by conditioning cancer cells and promoting angiogenesis. *J Exp Clin Cancer research: CR*. (2024) 43:160. doi: 10.1186/s13046-024-03082-z

55. Jiang D, He J, Yu L. The migrasome, an organelle for cell-cell communication. *Trends Cell Biol*. (2025) 35:205–16. doi: 10.1016/j.tcb.2024.05.003

56. Jha A, Chandra A, Farahani P, Toettcher J, Haugh JM, Waterman CM. CD44 and Ezrin restrict EGF receptor mobility to generate a novel spatial arrangement of cytoskeletal signaling modules driving bleb-based migration. *bioRxiv: preprint server Biol*. (2025). doi: 10.1101/2024.12.31.630838

57. Liu X, Jiao H, Zhang B, Zhang S, Yan K, Qu J, et al. Migrasomes trigger innate immune activation and mediate transmission of senescence signals across human cells. *Life Med*. (2023) 2:lnad050. doi: 10.1093/lifemedi/lnad050

58. Zhang X, Li J, Yao Y, Zhou M, He Y, Zhao Y. Migrasome-related prognostic signature TSPAN4 correlates with immune infiltrates and metabolic disturbances in hepatocellular carcinoma. *J gastroenterology*. (2025) 60:593–606. doi: 10.1007/s00535-025-02212-4

59. Huang Z, Wang M, Chen Y, Tang H, Tang K, Zhao M, et al. Glioblastoma-derived migrasomes promote migration and invasion by releasing PAK4 and LAMA4. *Commun Biol*. (2025) 8:91. doi: 10.1038/s42003-025-07526-w

60. Hirakawa T, Yashiro M, Doi Y, Kinoshita H, Morisaki T, Fukuoka T, et al. Pancreatic Fibroblasts Stimulate the Motility of Pancreatic Cancer Cells through IGF1/IGF1R Signaling under Hypoxia. *PloS One*. (2016) 11:e0159912. doi: 10.1371/journal.pone.0159912

61. Li M, Peng F, Wang G, Liang X, Shao M, Chen Z, et al. Coupling of cell surface biotinylation and SILAC-based quantitative proteomics identified myoferlin as a potential therapeutic target for nasopharyngeal carcinoma metastasis. *Front Cell Dev Biol*. (2021) 9:621810. doi: 10.3389/fcell.2021.621810

62. Bian Z, Chen J, Liu C, Ge Q, Zhang M, Meng J, et al. Landscape of the intratumroal microenvironment in bladder cancer: Implications for prognosis and immunotherapy. *Comput Struct Biotechnol J*. (2023) 21:74–85. doi: 10.1016/j.csbj.2022.11.052

63. Mondal C, Di Martino JS, Bravo-Cordero JJ. Actin dynamics during tumor cell dissemination. *Int Rev Cell Mol Biol*. (2021) 360:65–98. doi: 10.1016/bs.ircmb.2020.09.004

64. Zhang J, Lu S, Lu T, Han D, Zhang K, Gan L, et al. Single-cell analysis reveals the COL11A1(+) fibroblasts are cancer-specific fibroblasts that promote tumor progression. *Front Pharmacol*. (2023) 14:1121586. doi: 10.3389/fphar.2023.1121586

65. Chi H, Chen H, Wang R, Zhang J, Jiang L, Zhang S, et al. Proposing new early detection indicators for pancreatic cancer: Combining machine learning and neural networks for serum miRNA-based diagnostic model. *Front oncology*. (2023) 13:1244578. doi: 10.3389/fonc.2023.1244578

66. Wu IC, Chen YK, Wu CC, Cheng YJ, Chen WC, Ko HJ, et al. Overexpression of ATPase Na+/+ transporting alpha 1 polypeptide, ATP1A1, correlates with clinical diagnosis and progression of esophageal squamous cell carcinoma. *Oncotarget*. (2016) 7:85244–58. doi: 10.18632/oncotarget.13267

67. Chia PL, Ang KH, Thura M, Zeng Q. PRL3 as a therapeutic target for novel cancer immunotherapy in multiple cancer types. *Theranostics*. (2023) 13:1876–91. doi: 10.7150/thno.79265

68. Song J, Yang R, Wei R, Du Y, He P, Liu X. Pan-cancer analysis reveals RIPK2 predicts prognosis and promotes immune therapy resistance via triggering cytotoxic T lymphocytes dysfunction. *Mol Med (Cambridge Mass)*. (2022) 28:47. doi: 10.1186/s10020-022-00475-8

69. Wang LJ, Xu R, Wu Y. Migrasome regulator TSPAN4 shapes the suppressive tumor immune microenvironment in pan-cancer. *Front Immunol*. (2024) 15:1419420. doi: 10.3389/fimmu.2024.1419420

70. Zhou C, Liang Y, Zhou L, Yan Y, Liu N, Zhang R, et al. TSPAN1 promotes autophagy flux and mediates cooperation between WNT-CTNNB1 signaling and autophagy via the MIR454-FAM83A-TSPAN1 axis in pancreatic cancer. *Autophagy*. (2021) 17:3175–95. doi: 10.1080/15548627.2020.1826689

71. Shao S, Bu Z, Xiang J, Liu J, Tan R, Sun H, et al. The role of Tetraspanins in digestive system tumor development: update and emerging evidence. *Front Cell Dev Biol*. (2024) 12:1343894. doi: 10.3389/fcell.2024.1343894

72. Viktorsson K, Rieckmann T, Fleischmann M, Diefenhardt M, Hehlgans S, Rödel F. Advances in molecular targeted therapies to increase efficacy of (chemo)radiation therapy. *Strahlentherapie und Onkologie: Organ der Deutschen Rontgengesellschaft*. (2023) 199:1091–109. doi: 10.1007/s00066-023-02064-y

73. Liu T, Cheng S, Xu Q, Wang Z. Management of advanced pancreatic cancer through stromal depletion and immune modulation. *Medicina (Kaunas Lithuania)*. (2022) 58:1298. doi: 10.3390/medicina58091298

74. Choi B, Vu HT, Vu HT, Radwanska M, Magez S. Advances in the immunology of the host-parasite interactions in african trypanosomosis, including single-cell transcriptomics. *Pathog (Basel Switzerland)*. (2024) 13:188. doi: 10.3390/pathogens13030188

75. Zhao R, Pan Z, Qiu J, Li B, Qi Y, Gao Z, et al. Blocking ITGA5 potentiates the efficacy of anti-PD-1 therapy on glioblastoma by remodeling tumor-associated macrophages. *Cancer Commun (London England)*. (2025) 45:1–25. doi: 10.1002/cac2.70016

76. Kovaleva O, Sorokin M, Egorova A, Petrenko A, Shelekhova K, Gratchev A. Macrophage - tumor cell interaction beyond cytokines. *Front oncology*. (2023) 13:1078029. doi: 10.3389/fonc.2023.1078029